Inhibition of PIP4Kγ ameliorates the pathological effects of mutant huntingtin protein

Ismael Al-Ramahi[1], Sai Srinivas Panapakkam Giridharan[5], Yu-chi Chen[2], Samarjit Patnaik[2], Nathaniel Safren[6], Junya Hasegawa[5], Maria de Haro[1], Amanda K. Wagner Gee[2], Steve Titus[2], Hyunkyung Jeong[3], Jonathan Clarke[4], Dimitri Krainc[3], Wei Zheng[2], Robin F. Irvine[4], Sami Barmada[6], Marc Ferrer[2], Noel Southall[2], Lois S. Weisman[5]*, Juan Botas[1]*, Juan Jose Marugan[2]*

1. Baylor College of Medicine, Jan and Dan Duncan Neurological Research Institute, Texas Children's Hospital, 1250 Moursund, Houston, TX 77030
2. National Center for Advancing Translational Sciences, Division of Preclinical Innovation, 9800 Medical Center Drive, Rockville, MD, 20878
3. Northwestern University, The Ken and Ruth Davee Department of Neurology, Feinberg School of Medicine, 303 E. Chicago Ave, Ward 12-140, Chicago IL, 60611
4. University of Cambridge, Department of Pharmacology, Tennis Court Road, Cambridge CB2 1PD UK
5. University of Michigan, Department of Cell and Developmental Biology, Life Sciences Institute, Ann Arbor, MI 48109
6. University of Michigan, Department of Neurology, Ann Arbor, MI 48109

* co-corresponding authors

Abstract

The discovery of the causative gene for Huntington's disease (HD) has promoted numerous efforts to uncover cellular pathways that lower levels of mutant huntingtin protein (mHtt) and potentially forestall the appearance of HD-related neurological defects. Using a cell-based model of pathogenic huntingtin expression, we identified a class of compounds that protect cells through selective inhibition of a lipid kinase, PIP4Kγ. Pharmacological inhibition or knock-down of PIP4Kγ modulates the equilibrium between phosphatidylinositide (PI) species within the cell and increases basal autophagy, reducing the total amount of mHtt protein in human patient fibroblasts and aggregates in neurons**.** In two *Drosophila* models of Huntington's disease, genetic knockdown of PIP4K ameliorated neuronal dysfunction and degeneration as assessed using motor performance and retinal degeneration assays respectively. Together, these results suggest that PIP4Kγ is a druggable target whose inhibition enhances productive autophagy and mHtt proteolysis, revealing a useful pharmacological point of intervention for the treatment of Huntington's disease, and potentially for other neurodegenerative disorders.

Introduction

Huntington's disease (HD) is an autosomal dominant neurodegenerative disorder with no curative or preventative treatment options. The disease is caused by the expansion of a translated CAG trinucleotide repeat within exon 1 of the huntingtin gene (*HTT*), resulting in a mutant huntingtin (mHtt) protein with an abnormally long N-terminal tract of glutamine residues [1]. Individuals with more than 36 to 39 repeats develop the disorder, and the length of the repeat correlates with the age of disease onset [2]. The poly-glutamine repeat expansion impacts the physical [3] and physiological [4-6] properties of the huntingtin protein, producing aggregates in aged striatal neurons that eventually precipitate to form neuronal inclusion bodies [7]. Accumulation of mHtt triggers a variety of insults that lead to striatal degeneration, however, the nature of the specific mHtt species, soluble, oligomeric or aggregate, that triggers neurodegeneration remains unclear [8, 9]. In the last decade, a number of potential therapeutic avenues have been proposed to prevent or attenuate the neurodegeneration induced by mHtt, including examining the effects of mHtt-induced oxidative stress [10-12], huntingtin posttranscriptional modifications [13-16], microglia activation [17], a systematic exploration of coding [17] and non-coding [18] DNA, and autophagy [19, 20]. However, it has been difficult to identify druggable targets that reduce disease progression [21]. In addition to targeting mHtt-induced downstream pathogenic events, an attractive alternative for developing HD therapies is reducing the levels of mHtt protein, thus addressing pathogenesis at its root. The therapeutic potential of this approach is supported by observations in animal and cellular models of HD [19, 22-27]. Here we present PIP4Kγ as a novel therapeutic target for HD. PIP4Kγ [Phosphatidylinositol-5-phosphate 4-kinase, type II γ] is a lipid kinase expressed by the PIP4K2C gene. The protein is predominantly localized in several tissues, including the brain [28-31]. Enzymatically, PIP4Kγ phosphorylates phosphatidylinositol-5-phosphate [PI5P] to produce phosphatidylinositol 4,5-bisphosphate [PI(4,5)P2] [32]. The biological function of PIP4Kγ is not completely understood, although recent reports suggest a role in the modulation of vesicle trafficking [30], and mTOR signaling [33]. Recently we presented the first selective inhibitor of PIP4Kγ [34]. Here we introduce an additional chemotype with striking cell-based activity which prompted us to explore the utility of inhibiting PIP4Kγ in the context of pathologic mHtt expression. We show that inhibiting PIP4Kγ activity modulates productive autophagy, reduces mHtt protein levels in patient fibroblasts, and clears mHtt aggregates in neuronal cell models. Moreover, we show that inhibition of PIP4Kγ rescues mHtt-induced neurodegeneration in two *Drosophila* HD models.

Results

Identification of novel PIP4Kγ inhibitors

NCT-504 (Figure 1A) is an analogue obtained upon medicinal chemistry optimization of a series of 5-phenylthieno[2,3-d]pyrimidine compounds identified in a high-throughput phenotypic screen [35]. Expression of GFP-Htt(exon1)-Q103 in PC12 cells produces detergent-resistant GFP-labeled aggregates [36]. NCT-504 caused a robust reduction of GFP-Htt(exon1)-Q103 levels, as measured by lowered GFP signal (Figure 1B and 1C). NCT-504 treatment also decreased huntingtin aggregates in HEK293T cells transiently transfected with GFP-Htt(exon1)-Q74 (Figure 1 – figure supplement 1). As thienopyrimidines have been associated with kinase activity [37] we profiled NCT-504 against a panel of 442 human kinases http://www.discoverx.com/technologies-platforms/competitive-binding-technology/kinomescan-technology-platform. Using a cutoff of >65% inhibition at 10 μM, NCT-504 was active against only a single kinase, PIP4Kγ (Table 1). Similarly, another analogue from the same thienopyrimidine series, ML168 [35], had activity against six kinases in the same panel, but was most potent against PIP4Kγ.

To better characterize the biochemical action of NCT-504, we evaluated its inhibitory activity in several *in vitro* kinase assays. NCT-504 modulated the activity of PIP4Kγ in the DiscoverX® binding assay (https://www.discoverx.com/services/drug-discovery-development-services/kinase-profiling/kinomescan) with a Kd = 354 nM (Figure 1D). Using a reconstituted assay of phosphorylation of the PI5P substrate by full length PIP4Kγ, NCT-504 inhibited enzyme activity with an IC_{50} of 15.8 μM (Figure 1E). Notably, in the absence of PI5P substrate, the compound did not impair the intrinsic ATP-hydrolytic activity of PIP4Kγ (Figure 1F), suggesting that NCT-504 is an allosteric inhibitor of this kinase. This may account for the differences in potency observed in the enzymatic assay vs the DiscoverX® binding assay. Similar differences in potency between these two assays have also been observed for allosteric modulators of other kinases [38, 39]. NCT-504 function as an allosteric inhibitor may also explain why NCT-504 is exquisitely selective in the kinase profiling assay. In isolated enzyme assays against other PIP4K isoforms, 50 μM NCT-504 did not inhibit PIP4Kbeta or PIP4Kalpha (IC_{50} between 50 μM and 100 μM) (Figure 1 – figure supplement 2). We also characterized the compound using an alternate PIP4Kγ+ functional assay, which employs PIP4Kγ with a mutated G-loop and two additional mutations (described as PI5P4Kγ G3+AB in [40]) to increase the low intrinsic ATP turnover of the kinase in the presence of PI5P [40]. NCT-504 was largely inactive against PIP4Kγ+ with a potency >500 μM (Figure 1 – figure supplement 3).

PIP4Kγ inhibition modulates cellular phosphatidylinositide levels in complex ways

Cellular inhibition of PIP4Ks should impair the production of PI(4,5)P2 from PI5P, resulting in an elevation of PI5P cellular levels as previously described in the *Drosophila* mutant [41]. Note that other PI levels were not tested in the dPI4PK *Drosophila* mutant. We hypothesized that elevation of PI5P might further impact the equilibrium between various PI species [32, 42, 43]. To test this hypothesis, we exposed wild type mouse embryonic fibroblasts to nontoxic concentrations of NCT-504 (10 μM) for 12 hours, and then evaluated the levels of PI by HPLC

(Figure 2; toxicity assay in Figure 2-figure supplement 1). As expected, exposure to NCT-504 elevated cellular levels of PI5P (Figure 2D). Surprisingly, NCT-504 also robustly increased PI(3,5)P2 levels, and to a lesser extent increased levels of PI3P (Figure 2B and E). We did not observe an effect on PI(4,5)P2 levels (Figure 2F), which is consistent with other reports indicating that the cellular levels of this lipid are mostly generated from PI4P via type I PI4P 5-kinases [32]. Kinetic measurement of PI levels showed that NCT-504 causes an increase in PI5P, PI(3,5)P2 and PI3P levels along with a decrease in PI4P, progressively over 12 hours (Figure 2 – figure supplement 2). These statistically significant changes were not observed at 30 or 120 minutes suggesting that direct inhibition of PIP4Kγ eventually impacts other lipid kinases and phosphatases. Moreover treatment of unaffected human fibroblasts with NCT-504 elevated these three lipids in a dose dependent manner (Figure 2-supplement figure 3). Further evidence that the changes in PI levels are due to the specific inhibition of PIP4Kγ, is the finding that shRNA-mediated silencing of PIP4Kγ resulted in a similar PI profile to that observed with NCT-504 inhibition, namely an elevation of PI5P, PI(3,5)P2 and PI3P (Figure 2B, D and E). Note that during shRNA-mediated silencing of PIP4Kγ transcripts, PIP4Kγ protein was no longer detected (Figure 2G).

PIP4Kγ inhibition stimulates productive autophagy

Numerous studies have shown that mHtt upregulates autophagy, but impairs incorporation of client proteins into autophagosomes [44-48]. Importantly, a number of autophagy modulators have been described that reduce mHtt aggregates [19, 49-51]. That NCT-504 elevates the levels of three PI species implicated as positive regulators of autophagy suggests that the observed reduction in HTT-exon1-polyQ aggregates observed with NCT-504 treatment may occur due to upregulation of autophagy. Autophagy can be monitored by following the fate of microtubule-associated protein 1 light chain 3B (LC3-I). During autophagosome formation LC3-I gets conjugated to phosphatidylethanolamine to form LC3-II, which is degraded upon autophagosome-lysosome fusion [52]. We tested and found that a two hour incubation of HEK293T cells with 5 or 10 μM NCT-504 did not significantly increase LC3-II levels (Figure 3A and B). However, LC3-II levels depend on the rate of autophagosome formation, the rate of autophagosome-lysosome fusion, and on the rate of LC3-II degradation in mature autolysomes. Bafilomycin A1 inhibits the lysosomal v-ATPase, prevents autophagosome-lysosome fusion, and thus prevents autophagy-mediated degradation of LC3-II. Comparison of cells treated with and without bafilomycin A1 is a common method to monitor the rate of autophagosome formation within the cell independent of later steps [53]. Bafilomycin A1 treatment for 2 or 6 hours elevated the total amount of LC3-II (Figure 3A and C). Importantly, treating cells with 10 μM NCT-504 and 100 nM bafilomycin A1 for two hours and six hours resulted in a 38% and 51% increase in LC3-II levels respectively compared with bafilomycin A1 treatment alone, which indicates that NCT-504 induces autophagosome formation. Similarly, treating cells with 5 μM NCT-504 and bafilomycin A1 for two and six hours resulted in a 30% and 46% increase in LC3-II levels respectively. Importantly, an elevation in LC3-II levels by NCT-504 in the presence of bafilomycin A1 but not in the absence of bafilomycin A1, suggests that NCT-504 elevates both the induction of autophagy as well as the rate of turnover of autophagic cargo (autophagy flux). To further evaluate the effects of NCT-504 on autophagosome formation and autophagy flux,

we used a 293A cell line stably expressing a GFP-mCherry-LC3 reporter (Figure 3 – figure supplement 1). This double tagged LC3 is commonly used to distinguish between autolysosomes and autophagosomes or phagophores [54, 55]. Phagophore and autophagosome membranes conjugated with GFP-mCherry-LC3 are positive for both GFP- and mCherry-fluorescence. Upon generation of mature autolysosomes via fusion of autophagosomes with lysosomes, the GFP fluorescence from the internalized GFP-mCherry-LC3 is quenched in the acidic lysosomes; whereas mCherry fluorescence is insensitive to acidic pH and remains detectable. Thus, membrane structures positive for mCherry fluorescence, but not GFP fluorescence are autolysosomes. We determined the dose and time response of NCT-504 on autophagosomes and autolysosomes using GFP-mCherry-LC3; bafilomycin and torin-1 were used as controls (Figure 3 – figure supplement 1). As previously reported, bafilomycin treatment resulted in an increase in autophagosomes because the subsequent formation of autolysosomes is blocked. In addition, as previously reported, torin treatment elevated both the number of autophagosomes and autolysosomes, because inhibition of mTORC1 causes an increase in the induction of autophagy as well as an increase in autophagic flux. In contrast, NCT-504 treatment caused a robust increase in the formation of autolysosomes with only a modest elevation in autophagosomes, which indicates that NCT-504 increases autophagic flux, with only a modest increase in autophagy initiation.

While mechanisms of autophagy are highly similar in all cells, neurons exhibit some key differences. For example starvation does not upregulate autophagy [56]. In addition, autophagy is spatially regulated [57]. Thus, we tested whether NCT-504 impacts autophagy in neurons. We tested several doses and time points (up to 72 hours after treatment) and measured autophagy flux in DIV4 rat primary cortical neurons transfected with Dendra2-LC3, a photoconvertable reporter (Figure 3 – figure supplement 2). Dendra2 has excitation-emission maxima that are similar to GFP. However, exposure to intense blue light raise these maxima, and thus red light is emitted. Since the photoconversion reaction is irreversible, and LC3 is both a marker of autophagy as well as a substrate, the disappearance of red Dendra2-LC3 over time can be used to assess autophagy flux in a noninvasive manner [58, 59]. As a positive control for an increase in autophagic flux in neurons, we co-expressed Beclin-1, a positive regulator of autophagy that increases autophagy activity when overexpressed [60]. Importantly, treatment of rat primary cortical neurons expressing Dendra2-LC3 with either 500 nM or 1 μM NCT-504 enhanced the rate of Dendra2-LC3 turnover. Thus, NCT-504 stimulates autophagy flux in primary rodent cortical neurons in a statistically significant manner up to 72 hours following treatment.

That NCT-504-induced changes in autophagic flux were dose dependent, led us to test whether the resultant increase in autophagy correlated with changes in Htt levels. We found that 293A cells display a high content of wt Htt, which enabled us to use an anti-Htt FRET assay [61]. Using this assay, we found that NCT 504 treatment resulted in a dose dependent decrease of Htt protein levels at levels that did not impact cell viability (Figure 3 – figure supplement 1C and D).

To further test whether NCT-504 reduces mHtt aggregates via increasing autophagic flux, we tested the ability of NCT-504 to lower GFP-Htt(exon1)-Q74 aggregates in a cells with a defect in

macroautophagy. We found that while NCT-504 lowered the levels of GFP-Htt(exon1)-Q74 aggregates in Atg7+/+ MEF, it failed to lower aggregates in Atg7-/- MEF; Atg7 is essential for autophagosome formation and its loss inhibits the autophagy pathway (Figures 3 – figure supplement 3).

That PI3P is a critical regulator of autophagy [62], and that PI5P and PI(3,5)P2 have also been implicated in the autophagy process [63, 64], suggests that upregulation of one or more of these lipids is the driver behind the increase in autophagic flux. Importantly, NCT-504 treatment contrasts with the action of other autophagy modulators such as mTORC1 inhibitors which produce stable increases in LC3-II [65], accelerating the initiation of autophagy but not necessarily later steps which require mTOR reactivation [66].

Blocking PIP4Kγ activity reduces levels of full-length mutant huntingtin protein and levels of Htt(exon1)-polyQ aggregates

To test whether PIP4Kγ inhibition lowers full-length mHtt protein, we used immunoblots to determine the effect of NCT-504 on mHtt levels in patient fibroblasts and immortalized striatal neurons from a knock-in HD mouse model. Notably, treatment with 5 μM NCT-504 for 12 hour, conditions that did not affect cell viability (Figure 4 – figure supplement 1), significantly reduced mHtt levels in fibroblasts from two different HD patients HD(Q68) or HD(Q45) (Figure 4A and 4C). To further test whether the reduction of mHtt levels was due to selective modulation of PIP4Kγ, we individually silenced PIP4K2A, PIP4K2B and PIP4K2C RNA in the HD(Q68) patient fibroblast cell line. Only silencing of PIP4K2C exhibited an appreciable and robust reduction of huntingtin protein levels (Figure 4B). Note that silencing of PIP4K2A, PIP4K2B and PIP4K2C was effective and specific for each isoform (Figure 4 – figure supplement 2). We also tested the effect of NCT-504 on the levels of mutant full-length huntingtin protein in immortalized striatal neurons. We treated a striatal cell line from a knock-in HD mouse (ST*Hdh*Q111) [67], with 5 μM NCT-504 for 12 hours and observed a 40% decrease in mHtt levels (Figure 4D).

To examine the impact of NCT-504 on the levels of huntingtin-related aggregates in neurons, we evaluated the effect of NCT-504 in wild-type mouse primary cortical neurons transfected with Htt(exon1)-Q74. We tested and found that concentrations of NCT-504 of 5 μM or lower did not impact the viability of cortical neurons (Figure 4 – figure supplement 3). Importantly, 2.5 or 5 μM NCT-504 lowered the levels of Htt(exon1)-Q74 in primary cortical neurons (Figure 4 – figure supplement 4A). Moreover, depletion of PIP4Kγ in cortical neurons via PIP4K2C-shRNA treatment also led to a decrease in Htt(exon1)-Q74 levels and Htt(exon1)-Q74 aggregates (Figure 4 – figure supplement 4B). Furthermore, NCT-504 treatment and PIP4K2C silencing each reduced Htt(exon1)-polyQ aggregates in neuroblastoma N2a cells transfected with Htt(exon1)-polyQ mutants (Figure 4 – figure supplement 5).

Collectively, these studies show that NCT-504, a PIP4Kγ kinase inhibitor, at non-toxic concentrations, reduced full length huntingtin protein in patient fibroblasts, in immortalized striatal neurons from ST*Hdh*Q111 mutant mice and in HEK293T cells. Moreover, NCT-504 reduced the levels of Htt(exon1)-polyQ aggregates in primary cultured neurons and several cell lines. Similarly, specific silencing of the PIP4K2C gene led to reduction in the levels of full-length

huntingtin and HTT-exon1-polyQ protein and aggregates. The lowering of huntingtin and Htt(exon1)-polyQ by NCT-504 was concentration dependent. Moreover, the levels of NCT-504 that reduced these mutant proteins increased autophagic flux. Importantly, NCT-504 did not lower Htt(exon1)-polyQ protein in Atg7-/- MEF, but lowered Htt(exon1)-polyQ protein in the corresponding Atg7+/+ MEF. Together these studies indicate that inhibition of PIP4Kγ lowers mutant Htt, via an increase in autophagic flux.

Phenotypic effects of PIP4K modulation in *Drosophila* models of Huntington's Disease.

Unlike mammals, which have three PIP type II enzymes (PIP4Kalpha, PIP4Kbeta and PIP4Kγ), there is only one type II PIP kinase homologue in *Drosophila* (dPIPK4 also called CG17471) [33]. We used a well-established HD *Drosophila* model [68-72] to evaluate the impact of modulating the dPIP4K gene on the pathogenesis induced by mHtt expression. The GAL4/ UAS system [73] is used to drive expression of an N-terminal human 128Q mHtt (HttN231Q128) fragment to the cell type of choice. First, we assessed the *Drosophila* retina and its photoreceptor cells. Control HD model animals with wild-type activity of dPIP4K show prominent mHtt-induced photoreceptor degeneration. This phenotype is ameliorated by reducing dPIP4K activity with either one of two different shRNAs (Figure 5A). In a second set of experiments we tested the potential of dPIP4K to modulate mHtt pathogenesis using a behavioral readout. Neuronal-specific expression of HttN231Q128 leads to a late-onset motor impairment that can be quantified in a climbing assay. This phenotype was also ameliorated by reducing the activity of dPIP4K using a previously described [41] classical loss-of-function mutant allele in heterozygosis and a kinase dead allele (Figure 5B). Additionally, we also evaluated these approaches (loss-of-function by a heterozygous mutant allele and kinase dead allele) in animals expressing full length Htt carrying a 200 polyQ expansion in exon1. Notably, we observed a mitigation of the motor performance decline in this full-length HD model. Decreasing the levels of PIP4K with the same alleles in the absence of mHtt did not affect motor performance when compared to controls (Figure 5 - figure supplement 1). Thus, reducing the activity of dPIP4K using different genetic approaches mitigates mHtt pathogenesis in three different assays.

Discussion

Our unbiased screen for compounds that protect cells against a pathogenic huntingtin fragment reveal PIP4Kγ as a potential target for Huntington disease. The compounds identified led to the development of NCT-504, a selective fully efficacious inhibitor of PIP4Kγ. NCT-504 treatment or knock-down of PIP4Kγ lowers huntingtin fragments Htt(exon1)-polyQ in multiple cell types including cortical and striatal neurons, and lowers full-length mutant huntingtin in patient fibroblasts and mouse striatal neurons. Moreover, genetic targeting of PIP4K in two Drosophila models of HD, mitigated associated HD phenotypes. Importantly, we observed two major changes in cells following PIP4Kγ inhibition, an increase in autophagic flux, and an increase in the levels of three phosphoinositide signaling lipids. It is tempting to speculate that the changes in PI upregulate autophagic flux, and thereby lower mHtt levels.

Little is currently known about cellular roles of PIP4Kγ. However, in line with our current findings, previous studies observed that knock-down of PIP4Kγ resulted in an increase in autophagy [33, 63], and a reduction of EGFP-HttQ74 aggregates in MEFs that was dependent on the presence of the autophagy gene, ATG7 [33, 63].

While increasing the proteolysis of pathogenic huntingtin protein via the upregulation of autophagy is an attractive therapeutic approach for HD [26, 27], there are potential challenges. Mutant huntingtin itself may alter autophagy. Wild-type huntingtin may be an adaptor for selected autophagic cargoes including itself [47]. Consistent with this hypothesis, mutant huntingtin impairs the loading of ubiquitinated-tagged proteins into autophagosomes [47], and circumvents its own clearance [46]. Moreover, mutant huntingtin sequesters diverse proteins required for key cellular processes [74], including mTOR, which plays key roles in the regulation of autophagy [48, 75-80]. In addition, the PI binding autophagy adaptor protein ALFY which plays a fundamental role in degrading mutant huntingtin is down-regulated in HD [46, 81]. In contrast with these findings, their studies indicate that autophagy is not impaired in HD, and have revealed an elevation of autophagy flux in HD cells [75, 82]. Despite possible mutant huntingtin-dependent changes on autophagy, upregulation of autophagy remains a viable approach for lowering levels of mutant huntintin and aggregates [26, 27]. Note that caloric restriction also raises the basal level of autophagy, leading to improvements in HD models [83] and increasing axonal autophagosome transport [84], although it is less clear how to translate this observation into clinical practice.

One common approach to induce autophagy is via inhibition of the major metabolic kinase mTORC1. Indeed, rapamycin, an inhibitor of mTORC1 also reduces mHtt protein levels [19]. However, while PIP4Kγ likely impacts mTORC1 activity, it is not yet clear whether PIP4Kγ inhibition results in mTORC1 inhibition or activation. One study showed that knock-down of PIP4K2C inhibits mTORC1 [33]. However, in PIP4K2C homozygous knock-out mice, mTORC1 is elevated [85]. Thus, the precise link between PIP4Kγ and mTORC1 is not clear. Importantly, our data suggest that PIP4Kγ upregulation of autophagy has some differences with upregulation of autophagy via mTORC1 inhibition. While inhibition of mTOR via torin treatment exhibited a large increase in both autophagosome formation and autophagy flux, inhibition of PIP4Kγ had only a modest impact on autophagosome formation, but had a large increase in autophagic flux

(Figure 3 – figure supplement 1). Thus, elucidation of the mechanism whereby PIP4Kγ inhibition increases autophagic flux remains to be fully determined.

It is likely that inhibition of PIP4Kγ increases autophagic flux at least in part via the resulting impact on the levels of selected phosphoinositide lipids. PIP4Kγ is predicted to convert PI5P to PI(4,5)P2. However, it was not known which cellular pools of PI5P are substrates for PIP4Kγ. Using NCT-504 we found no significant change in PI5P levels or other PI lipids following up to two hours of inhibition of PIP4Kγ. This contrasts with other lipid kinases such as PIKfyve, where direct inhibition results in an acute loss of PI(3,5)P2 which can be observed within 5 min [86, 87]. The long delay prior to changes in PI5P following PIP4Kγ inhibition suggests that PIP4Kγ is not in contact with most of the cellular PI5P, or is only active under specific conditions. However, after 12 hour treatment with NCT-504, there was a 1.6 fold elevation of PI5P. The fact that this change occurred well after 2 hour of inhibition, suggests that it might not be directly due to an accumulation of the PI5P substrate normally used by PIP4Kγ. Indeed, at 12 hours PI(3,5)P2 levels were also elevated at 2-fold,which was even higher than the fold elevation in PI5P. This raises the possibility that long-term inhibition of PIP4Kγ indirectly results in the activation of PIKfyve. This activation of PIKfyve may account for the increase in PI5P as well as PI(3,5)P2 [86, 87] [88]. In addition, at 12 hour PI3P levels increased 1.3 fold, suggesting that VPS34 may be indirectly activated as well.

The elevation of PI3P, PI(3,5)P2 and/or PI5P likely contribute to the elevation in autophagic flux. PI3P has well characterized roles in autophagy, and acts in initiation of phagophore formation [62] as well as in later steps of autophagosome maturation [89], including autophagosome-lysosome fusion [90] and lysosome reformation [91, 92]. In some conditions, PI5P can induce autophagy independent of PI3P [63]. In contrast, PI(3,5)P2 functions at a late step in autophagy [90, 93-96] [97-99]. These late functions, may contribute to the observed increase in autophagic flux. In addition to these changes the statistically significant decrease in PI4P may also contribute to changes in autophagy. A reduction of PI4P has been postulated to be necessary for lysosome reformation [91, 92].

The elevation of PI3P, PI(3,5)P2 and PI5P may also have a role in compensating potential mutant huntingtin-dependent changes in PI or masking of selected PI. Several studies have indicated that there are polyglutamine-dependent alterations in PI binding of huntingtin protein [100-103]. Moreover, wild-type huntingtin binds phosphoinositide lipids including PI5P and PI(3,5)P2 [102]. Notably, when assessed using unilamellar vesicles, huntingtin with a polyglutamine expansion bound these lipids even more tightly than wild-type hungtingtin, potentially reducing the free total levels of these lipids and impacting their downstream dependent signaling [104]. Masking of PI lipids could negatively and progressively impact the function of proteins involved in autophagosome cargo recognition and loading, especially those effector proteins dependent on low abundance PI, such as PI5P and PI(3,5)P2. Additional studies need to be carried out to determine the effectors proteins (Alfy and/or others) responsible for the action of PIP4Kγ modulation, the mechanism of action behind the high cellular alteration in PI(3,5)P2 as well as the modulation of other PI levels, and the impact of those changes on mTOR function and autophagy dynamics [90, 95, 96]. It has not escaped our

attention that mHtt-dependent effects seem to be triggered by aging, which is known to limit the clearance of misfolded proteins [105], and deregulate phosphatidylinositide lipid signaling [106].

The data presented in this manuscript demonstrates that pharmacological inhibition, or knock-down of PIP4Kγ produce a similar reduction in huntingtin levels, and a concomitant elevation of PI5P and PI(3,5)P2 and PI3P. These findings open the door to a new disease-modifying approach for this disorder and validate PIP4Kγ as a druggable target. In a recent report, a homozygous mouse knockout displayed no growth or behavioral abnormalities [85]. From the translational point of view, the development of selective PIP4Kγ inhibitors could be extraordinarily useful for other neurodegenerative diseases as well. Alzheimer's disease and Parkinson's disease in particular are also mediated by the accumulation of toxic protein aggregates, whose catabolism by autophagy might rescue stressed neurons. Starvation increases life spans across species [107] and there are numerous diseases where upregulation of basal autophagy is beneficial [108, 109]. Further, dose response studies are necessary to fully evaluate the therapeutic potential of PIP4Kγ inhibition.

Materials and Methods

Synthesis of NCT-504

General Experimental Procedure: Unless otherwise stated, all reactions were carried out under an atmosphere of dry argon or nitrogen in dried glassware. Indicated reaction temperatures refer to those of the reaction bath, while room temperature is noted as ~25 °C. All anhydrous solvents, commercially available starting materials, and reagents were purchased from Aldrich Chemical Co. and used as received. Chromatography on silica gel was performed using forced flow (liquid) of the indicated solvent system on Biotage KP-Sil pre-packed cartridges and using the Biotage SP-1 automated chromatography system.

^{1}H spectra were recorded on a Varian Inova 400 MHz spectrometer. Chemical shifts are reported in ppm with the solvent resonance as the internal standard (DMSO-d_6 2.50 ppm, for 1H). Data are reported as follows: chemical shift, multiplicity (s = singlet, d = doublet, t = triplet, q = quartet, br s= broad singlet, m = multiplet), coupling constants, and number of protons.

Analytical purity analysis and retention times (RT) reported here were performed on an Agilent LC/MS (Agilent Technologies, Santa Clara, CA). A Phenomenex Luna C18 column (3 micron, 3 x 75 mm) was used at a temperature of 50 °C. The solvent gradients are mentioned for each compound and consist of a percentage of acetonitrile (containing 0.025% trifluoroacetic acid) in water (containing 0.05% trifluoroacetic acid). A 4.5 minute run time at a flow rate of 1 mL/min was used.

Mass determination was performed using an Agilent 6130 mass spectrometer with electrospray ionization in the positive mode.

Synthetic scheme to prepare NCT-504:

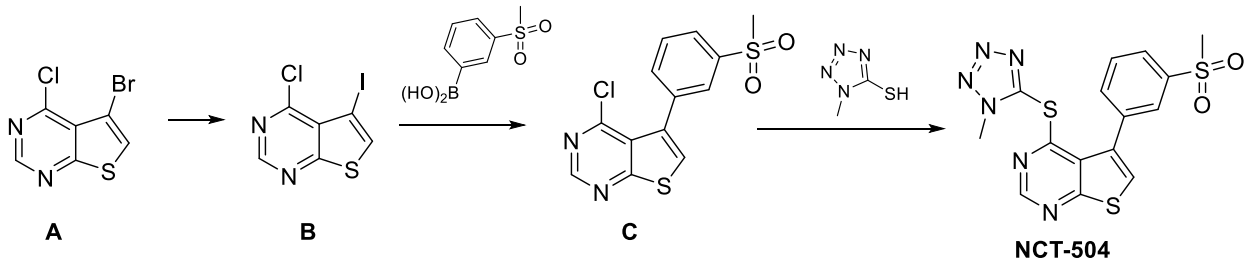

Synthetic Procedures:

B: **A** (5-bromo-4-chlorothieno[2,3-d]pyrimidine) was prepared according to WO2012/44993 A1, 2012 ; Location in patent: Page/Page column 45). A solution of **A** (1.03 g, 4.13 mmol) in THF (15 ml) was treated at 0 °C under nitrogen with dropwise addition of isopropylmagnesium chloride (2.48 ml, 4.95 mmol, 2M in THF). The mixture was stirred for 15 min and then a solution of iodine (1.05 g, 4.13 mmol) in THF (10 mL) was added dropwise under nitrogen. The mixture was stirred at 0 °C for almost 2 h, quenched with saturated aqueous NH_4Cl and then

EtOAc was added. The mixture was stirred, the organic layer was separated, washed with saturated aqueous $Na_2S_2O_3$, dried with $MgSO_4$, filtered, concentrated to obtain crude 4-chloro-5-iodothieno[2,3-d]pyrimidine (1.17 g, 3.95 mmol, 96% yield). This appeared to be contaminated with a small amount of **B** 4-chlorothieno[2,3-d]pyrimidine (approximately ~5-10% by LC/MS).

1H NMR (400 MHz, DMSO-d_6) δ 8.96 (s, 1H), 8.46 (s, 1H).

LC/MS Gradient 4% to 100% Acetonitrile (0.05% TFA) over 3.0 minutes; RT 3.290 min, ESI (M+1)+ calculated 296.9, found 296.8.

C: A microwave vial filled was charged with 4-chloro-5-iodothieno[2,3-d]pyrimidine **B** (0.48 g, 1.62 mmol), (3-(methylsulfonyl)phenyl)boronic acid (0.389 g, 1.94 mmol), $Pd(PPh_3)_4$ (0.094 g, 0.081 mmol), sodium carbonate (1.42 ml, 2.83 mmol) followed by dimethoxyethane (8 mL) and water (1 mL). The mixture was heated in the microwave under "high" settings at 120 ℃ for 20 min in the microwave. The mixture was then cooled; celite was added, and concentrated. The adsorbed material was purified by flash silica gel chromatography with a gradient of 0 to 30% EtOAc in DCM that separated unreacted starting iodide (~20% recovery) from the required product 4-chloro-5-(3-(methylsulfonyl)phenyl)thieno[2,3-d]pyrimidine C (0.19 g, 0.59 mmol, 36% yield).

1H NMR (400 MHz, DMSO-d_6) δ 9.02 (d, J = 0.4 Hz, 1H), 8.19 (d, J = 0.4 Hz, 1H), 8.08 (td, J = 1.8, 0.5 Hz, 1H), 8.02 (ddd, J = 7.8, 1.9, 1.1 Hz, 1H), 7.90 (ddd, J = 7.7, 1.7, 1.2 Hz, 1H), 7.77 (td, J = 7.7, 0.5 Hz, 1H), 3.29 (s, 3H). LC/MS Gradient 4% to 100% Acetonitrile (0.05% TFA) over 3.0 minutes, RT 3.014 min, ESI (M+1)+ calculated 325.0, found 324.9.

NCT-504: 4-Chloro-5-(3-(methylsulfonyl)phenyl)thieno[2,3-d]pyrimidine C (0.18 g, 0.55 mmol) with DME (10 mL) was treated with 1-methyl-1H-tetrazole-5-thiol (0.084 g, 0.720 mmol) and Hunig's Base (0.194 mL, 1.11 mmol), and heated at 120 ℃ for 30 min in a sealed tube. The mixture was cooled, concentrated, re-dissolved in minimal DCM and the purified by silica gel column chromatography (5 to 60% EtOAc/DCM) to provide NCT-504 4-((1-methyl-1H-tetrazol-5-yl)thio)-5-(3-(methylsulfonyl)phenyl)thieno[2,3-d]pyrimidine (190 mg, 0.470 mmol, 85 % yield).

1H NMR (400 MHz, DMSO-d_6) δ 8.76 (d, J = 0.4 Hz, 1H), 8.23 (td, J = 1.8, 0.5 Hz, 1H), 8.15 (d, J = 0.4 Hz, 1H), 8.10 (ddd, J = 7.8, 1.9, 1.1 Hz, 1H), 8.02 (ddd, J = 7.7, 1.7, 1.1 Hz, 1H), 7.86 (td, J = 7.8, 0.6 Hz, 1H), 3.96 (s, 3H), 3.34 (s, 3H).

LC/MS Gradient 4% to 100% Acetonitrile (0.05% TFA) over 3.0 minutes, RT 3.024 min, ESI (M+1)+ calculated 405.0, found 405.0.

Enzyme preparation and biochemical assays

Protein from human *PIP4K2A* (UniGene 138363), *PIP4K2B* (Unigene 269308) and *PIP4K2C* (UniGene 6280511) was expressed in pGEX6P (GE Healthcare) and purified from *E. coli* BL21(DE3). GST fusion proteins from cell lysates were bound to glutathione sepharose beads (GE Healthcare) and cleaved *in situ* with 50U of PreScission protease (GE Healthcare) for 4 hours at 4^{o}C.

Lipid kinase assays were performed essentially as described previously [110, 111]. In brief, dried substrate lipid (6 μM PI5P final reaction concentration) was resuspended in kinase buffer (50 mM Tris pH 7.4, 10 mM $MgCl_2$, 80 mM KCl, and 2 mM EGTA) and micelles were formed by sonication for 2 min. Recombinant lipid kinase, preincubated with inhibitor for 10 min on ice (where required), was added to the micelles and the reaction started by the addition of 10 μCi [^{32}P]ATP (200μl final volume), and incubated at 30℃ for 10-60 min (dependent on isoform). Lipids were extracted using an acidic phase-separation [112] and separated by one-dimensional thin layer chromatography (2.8:4:1:0.6 chloroform:methanol:water:ammonia). Radiolabelled PI(4,5)P2 product was detected by autoradiography, extracted from the plate and Cerenkov radiation was counted in the presence of Ultima Gold XR scintillant (Packard) on a LS6500 scintillation counter (Beckman Coulter). Specific enzyme activities, under these assay conditions, were calculated as nmoles of PI5P converted into PI(4,5)P2 per minute per mg of purified recombinant enzyme.

Intrinsic ATPase activities of the enzymes were determined using the Transcreener ADP^2 fluorescence polarization assay (BellBrook Labs). PIP4Kγ (1μM, [40]) was pre-incubated (10 min on ice) at range of inhibitor concentrations and assayed with ATP substrate (100 μM ATP, 60 min incubation at 22℃) in the absence of lipid substrate. Polarization units (mP) were read using a PHERAstar Plus microplate reader (BMG Labtech). Experimental values were interpolated from an ADP/ATP utilization standard curve and plotted using nonlinear regression analysis with Prism 5 (GraphPad).

Measurement of phosphorylated phosphoinositide (PI) levels by HPLC

PI measurements were performed as previously described [86]. Briefly, mouse primary fibroblasts were generated from P1 pups (129P2/OlaHsd × C57BL/6) and were cultured in DMEM supplemented with 15 % FBS and 1X Pen-Strep-Glutamine and human patient fibroblast were cultured in MEM supplemented with 15% FBS, 1x Pen-Strep and 1x Glutamax in 100 mm dishes to 60-70% confluence. MEF cells and patient fibroblasts were tested using MycoFluor™ Mycoplasma Detection Kit (Thermo Scientific Fisher) and were negative for mycoplasma contamination. Cells were washed with PBS and incubated with inositol labeling medium (containing custom-made inositol-free DMEM (11964092; Life Technologies), 10 μCi/mL of myo-^{3}H-inositol (GE Healthcare), 10% dialyzed FBS (26400; Life Technologies), 20 mM Hepes, pH 7.2-7.4, 5 μg/mL transferrin (0030124SA; Invitrogen), and 5 μg/mL insulin (12585-014; Invitrogen) for 48 hours. For experiments with NCT-504 treatments, cells were treated with indicated concentrations of NCT-504 or DMSO for indicated duration before the end of the labeling. Extraction and HPLC measurements were performed as described [86].

Silencing of PIP4Kγ

Primary mouse embryonic fibroblast cells generated from P1 pups (129P2/OlaHsd × C57BL/6) were infected with MISSION shRNA lentiviral plasmid pLKO.1-puro with shRNA target sequence CTCCAAGATCAAGGTCAACAA (TRCN0000024702; Sigma) containing 237-257 nucleotides of mouse PIP4Kγ cDNA; MISSION nontarget shRNA lentiviral control vector SHC002 (Sigma) was used as control. Transduction-ready viral particles were produced by the

Vector Core (University of Michigan, Ann Arbor, MI) with a concentration of 10^7 transduction units per ml. Mouse primary fibroblast grown on two 35 mm dishes were treated at an MOI of 5. After overnight incubation, cells were treated with 2 μg/ml puromycin. After two days of infection, cells from two 35 mm dishes were transferred to a 100 mm dish and maintained in puromycin containing media for another three days. Cells were either analyzed by western blot or incubated with inositol labeling medium for 48 hours for PI measurements. Immunoblots were performed with antibodies against PIP4K2C (17077-1-AP RRID: AB_2715526, ProteinTech; 1:5000) and GADPH (AM4300 RRID: AB 437392, Thermo Scientific Fisher; 1:50000).

LC3 Measurements in HEK cells

HEK 293T cells grown on 35 mm Dishes till 60-70% confluency were either untreated or treated with DMSO or NCT-504 with or without 100 nM Bafilomycin for two hours. Cells were lysed and immunoblotted with antibodies against LC3A/B (12741 RRID:AB_2617131; Cell Signaling) and α-tubulin (A-11126 A11126 RRID:AB_221538; Life Technologies). Blots were analyzed using Adobe Photoshop. HEK293T cells were purchased from ATCC (RRID:CVCL_0063) and were certified authentic and mycoplasma free.

Htt HTRF® assay

Antibodies: The monoclonal antibodies used in the HTRF® assay were 2B7 (gift from collaborator) which binds to the first 17 amino acids of normal and mutant Htt, and MAB2166 (EMD Milipore #MAB2166), which binds to an Htt epitope (amino acid 181 to 810), and recognizes both normal and mtHtt. The antibody 2B7 was conjugated to Tb as a donor, and 2166 was conjugated to d2 as an acceptor (both were custom labeled by Cisbio). The labeled antibody pairs were diluted in the 1X HTRF assay buffer: 50 mM NaH_2PO_4, 400 mM NaF, 0.1%BSA, 0.05% Tween 20. The HTRF assay were performed at 1536-well plate. For the experiments, cells were seeding (6μL/well) 24 hr in advanced and culture at 37 ºC 5%CO_2 followed by compound addition (23 nL). After incubating with compounds for 24 hr, cells were lysed by adding 2 μL of 4x lysis buffer (Cisbio Lysis buffer #2), incubated at room temperature for 2 hrs then add labeled antibodies. The labeled antibody pairs were diluted in the 1X HTRF assay buffer: 50 mM NaH_2PO, 400 mM NaF, 0.1%BSA, 0.05% Tween 20. The final reaction is 8μL/well. The signal ratio between 665 nm and 615 nm have been calculated as the raw HTRF ratio. The cell viability was measured by using CellTiter-Glo® Luminescent Cell Viability Assay (Promega). The 293A cells were purchased from ThermoFisher Scientific, Cat#R70507, Lot # 1657360. They tested negative for mycoplasma. They were not sent out for STR since it was first use right after purchase from company.

Htt exon1 aggregation assay

GFP-Htt-exon1-Q23 (Plasmid #40261)1 and GFP-Htt-exon1-Q74 (Plasmid #40262)1 were purchased from Addgene (Cambridge, MA) [113]. Immortalized Atg7+/+ and Atg7-/- MEF cells

were generously provided by Dr. Masaaki Komastu (School of medicine, Niigata University) [114]. Atg7+/+ and Atg7-/- MEF cells were tested using MycoFluor™ Mycoplasma Detection Kit (Thermo Scientific Fisher) and are negative for mycoplasma contamination. They were validated for the presence and absence, respectively, of Atg7 by the western blot shown in Figure 3C. These cell lines are not included in the list of commonly misidentified cell lines maintained by International Cell Line Authentication Committee were not authenticated further. HEK293T, Atg7+/+ and Atg7-/- cells grown on coverslips were transfected with either GFP-Htt-exon1-Q23 or GFP-Htt-exon1-Q74 using Lipofectamine® 2000 (Invitrogen). After 2 hours of transfection, cells were incubated with DMSO or 2 μM of NCT-504 for 48 hours and fixed. Transfected cells with mHtt aggregates were quantified [113, 114].

HTT quantification in Fibroblasts and StHdh cells

Immortalized StHdhQ111 (Coriell-CH00095, RRID:CVCL_M591) cells [67], immortalized wild type (Coriell-GM02153) and HDQ45 (Coriell-GM03868, RRID:CVCL_1H73) HD fibroblasts ((using SV40 large T antigen) [71] and non-immortalized HDQ68 (Coriell-GM21757, RRID:CVCL_1J85) were grown in 15%FBS DMEM with GlutaMax (Life Technologies). For drug treatments, cells were plated overnight until they reached 70% confluence in 12-well plates, drug was added at the desired concentration for 48 hours. For siRNA treatment cells were nucleofected using Amaxa at a final concentration of 30 nM and grown in 6-well plates for 72 hours. StHdh cells were grown in DMEM (Life Technologies) 10% FBS and drug treatment was carried out as described above. Cell identity was confirmed using STR profiling (GenePrint® 10 System from Promega Corp.) and tested mycoplasma negative (Hoechst staining).

Cells were collected using trypsin, homogenized in RIPA buffer, sonicated and incubated in ice for 30 minutes. Supernatant was collected after a 10 minutes centrifugation and protein concentration was measured. For western blot analysis 15 μg of each protein sample was loaded in a 4-12% Bis-tris gel, transferred into a nitrocellulose membrane, blocked with 5% milk and incubated overnight with anti-Huntingtin antibody MAB5492 (Millipore) for fibroblasts or MAB2166 (Millipore) for StHdhQ111 cells.

Ethical treatment of animals

All vertebrate animal work was approved by the Institutional Animal Use & Care Committee at the University of Michigan (PRO00007096). Experiments were carefully planned to minimize the number of animals needed. Pregnant female wild-type, non-transgenic Long Evans rats (*Rattus norvegicus*) were housed singly in chambers equipped with environmental enrichment. They were fed ad libitum a full diet (30% protein, 13% fat, 57% carbohydrate; full information available at www.labdiet.com), and cared for by the Unit for Laboratory Animal Medicine (ULAM) at the University of Michigan. Veterinary specialists and technicians in ULAM are trained and approved in the care and long-term maintenance of rodent colonies, in accordance with the NIH-supported Guide for the Care and Use of Laboratory Animals. All rats were kept in routine housing for as little time as possible prior to euthanasia and dissection, minimizing any pain and/or discomfort. Pregnant dams were euthanized by CO2 inhalation at gestation day 20. For each animal, euthanasia was confirmed by bilateral pneumothorax. Euthanasia was fully consistent with the recommendations of the Guidelines on Euthanasia of the American

Veterinary Medical Association and the University of Michigan Methods of Euthanasia by Species Guidelines. Following euthanasia, the fetuses were removed in a sterile manner from the uterus and decapitated. Primary cells from these fetuses were dissected and cultured immediately afterwards.

Rodent primary neuron isolation and culturing Primary mixed cortical neurons were dissected from these embryos as described previously [115], and plated in a poly-l-lysine/laminin coated 96 well plate at a density of 5 X 10^5 cells/ml. On day 4 *in vitro*, cells were transfected with Dendra2-LC3 with or without GFP-Beclin using Lipofectamine 2000 (Invitrogen). Thirty minutes post-transfection, neurons were treated with NCT-504 or DMSO. Optical pulse labeling experiments were performed as previously described [48, 58, 59]. Briefly, Dendra2-LC3 was photoconverted 24 hours post-transfection by illuminating each imaging field with a 250ms pulse of 405nm light. Following photoconversion, neurons were longitudinally imaged using a custom-built automated fluorescence microscopy platform [8, 59, 116]. A Nikon Eclipse Ti inverted microscope equipped with a high-NA 20X objective lens, a PerfectFocus3 system, and an Andor iXon3 897 EMCCD camera were used for image acquisition. GFP and TRITC images were taken immediately after photoconversion and four more times within the following 48 hours. Single-cell TRITC intensity values were fitted to a first-order exponential decay curve, generating a half-life value for each individual neuron. Neuronal survival analysis was assessed using original software written in Python. Only cells that lived the duration of imaging were included in the Dendra2-LC3 half-life analysis. Half-life was determined by fitting the TRITC intensity values at each time point to a first-order exponential function using scripts written in R. Comparisons between groups to determine statistical significance were accomplished using one-way ANOVA with Dunnet's post hoc test and the Kruskal-Wallis test.

***Drosophila* experiments**

Two different *Drosophila* HTT-expressing strains were used for this study, and N-terminal model expressing the first 336 amino acids of human HTT with a 128Q expansion [58] and a full length model expressing human HTT with a Q200 expansion [117]. For retinal expression, we used the GMR-GAL4 driver at 25C and for panneuronal expression, we used the elav-GAL4 driver. These two drivers as well as the siRNAs targeting dPIP4K were obtained from the Bloomington *Drosophila* stock center. The dPIP4K-29 loss of function allele and the K271D kinase dead (PIP4K-DN) allele were previously described and kindly provided by Dr. Padinjat Raghu [41].

For the retinal degeneration assay, animals were fixed with 4% formaldehyde in PBS. Heads were dehydrated in increasing concentrations of ethanol and embedded in paraffin. Ten µm serial sections were obtained and re-hydrated to PBS. Sections were stained with hematoxylin (SIGMA). Images were captured using an AxioCam MRc camera (ZEISS) attached to a MICROPHOT-FXA microscope (Nikon).

Motor performance of animals was assessed as a function of age. For the N-terminal model 15 age-matched virgin females per replica were used. Animals are taped to the bottom of a plastic vial and the number of animals reaching a height of 9 cm in 15 seconds is assessed using

infrared sensors. Ten trials are carried out for each day represented. The plotted data corresponds to the average percentage of animals reaching 9 cm. Data was analyzed by ANOVA followed by Dunnet's post hoc test. For the FL-HTTQ200 a similar procedure was used, the animals were video recorded and data was processed using a custom designed analysis software (source code file 1), which allowed for calculating speed.

Acknowledgements

Immortalized MEF wild-type and MEF Atg7 knock-out cells were a gift from Dr. Masaki Komatsu (Niigata University, Japan). None of the cell lines used in this study were included in the list of commonly misidentified cell lines maintained by International Cell Line Authentication Committee. This work was supported in part by National Institutes of Health (NIH) grants R01-NS064015 and R01-NS099340 to LSW, R01-NS097542 and P30-AG053760 to SJB, and the Protein Folding Diseases Fast Forward Initiative, University of Michigan to LSW and SJB. SSPG was supported in part by AHA Postdoctoral Fellowship, 14POST20480137. IA was supported by R21NS096395 grant from the NIH and by the Darrell K Royal Research Fund for Alzheimer's Disease. JB was supported by grants from the CHDI and the Robert A. and Renée E. Belfer Family Foundation.

References

1. Ross, C.A. and S.J. Tabrizi, *Huntington's disease: from molecular pathogenesis to clinical treatment.* Lancet Neurol, 2011. **10**(1): p. 83-98.
2. Walker, F.O., *Huntington's disease.* Lancet, 2007. **369**(9557): p. 218-28.
3. Kazantsev, A., et al., *Insoluble detergent-resistant aggregates form between pathological and nonpathological lengths of polyglutamine in mammalian cells.* Proc Natl Acad Sci U S A, 1999. **96**(20): p. 11404-9.
4. Hipp, M.S., et al., *Indirect inhibition of 26S proteasome activity in a cellular model of Huntington's disease.* J Cell Biol, 2012. **196**(5): p. 573-87.
5. Verhoef, L.G., et al., *Aggregate formation inhibits proteasomal degradation of polyglutamine proteins.* Hum Mol Genet, 2002. **11**(22): p. 2689-700.
6. Fernandez-Estevez, M.A., et al., *Trehalose reverses cell malfunction in fibroblasts from normal and Huntington's disease patients caused by proteosome inhibition.* PLoS One, 2014. **9**(2): p. e90202.
7. Miller, J., et al., *Quantitative relationships between huntingtin levels, polyglutamine length, inclusion body formation, and neuronal death provide novel insight into huntington's disease molecular pathogenesis.* J Neurosci, 2010. **30**(31): p. 10541-50.
8. Arrasate, M., et al., *Inclusion body formation reduces levels of mutant huntingtin and the risk of neuronal death.* Nature, 2004. **431**(7010): p. 805-10.
9. Lajoie, P. and E.L. Snapp, *Formation and toxicity of soluble polyglutamine oligomers in living cells.* PLoS One, 2010. **5**(12): p. e15245.
10. Wyttenbach, A., et al., *Heat shock protein 27 prevents cellular polyglutamine toxicity and suppresses the increase of reactive oxygen species caused by huntingtin.* Hum Mol Genet, 2002. **11**(9): p. 1137-51.
11. Giuliano, P., et al., *DNA damage induced by polyglutamine-expanded proteins.* Hum Mol Genet, 2003. **12**(18): p. 2301-9.
12. Lu, X.H., et al., *Targeting ATM ameliorates mutant Huntingtin toxicity in cell and animal models of Huntington's disease.* Sci Transl Med, 2014. **6**(268): p. 268ra178.
13. Steffan, J.S., et al., *SUMO modification of Huntingtin and Huntington's disease pathology.* Science, 2004. **304**(5667): p. 100-4.
14. Greiner, E.R. and X.W. Yang, *Huntington's disease: flipping a switch on huntingtin.* Nat Chem Biol, 2011. **7**(7): p. 412-4.
15. Bhat, K.P., et al., *Differential ubiquitination and degradation of huntingtin fragments modulated by ubiquitin-protein ligase E3A.* Proc Natl Acad Sci U S A, 2014. **111**(15): p. 5706-11.
16. Pavese, N., et al., *Microglial activation correlates with severity in Huntington disease: a clinical and PET study.* Neurology, 2006. **66**(11): p. 1638-43.
17. Gusella, J.F. and M.E. MacDonald, *Huntington's disease: the case for genetic modifiers.* Genome Med, 2009. **1**(8): p. 80.
18. Zhang, Y. and R.M. Friedlander, *Using non-coding small RNAs to develop therapies for Huntington's disease.* Gene Ther, 2011. **18**(12): p. 1139-49.
19. Sarkar, S., et al., *Rapamycin and mTOR-independent autophagy inducers ameliorate toxicity of polyglutamine-expanded huntingtin and related proteinopathies.* Cell Death Differ, 2009. **16**(1): p. 46-56.
20. Williams, A., et al., *Novel targets for Huntington's disease in an mTOR-independent autophagy pathway.* Nat Chem Biol, 2008. **4**(5): p. 295-305.
21. Bard, J., et al., *Advances in huntington disease drug discovery: novel approaches to model disease phenotypes.* J Biomol Screen, 2014. **19**(2): p. 191-204.

22. King, M.A., et al., *Rapamycin inhibits polyglutamine aggregation independently of autophagy by reducing protein synthesis.* Mol Pharmacol, 2008. **73**(4): p. 1052-63.
23. Singh, M.D., K. Raj, and S. Sarkar, *Drosophila Myc, a novel modifier suppresses the poly(Q) toxicity by modulating the level of CREB binding protein and histone acetylation.* Neurobiol Dis, 2014. **63**: p. 48-61.
24. Giorgini, F., *Is modulating translation a therapeutic option for Huntington's disease?* Neurodegener Dis Manag, 2011. **1**(2): p. 89-91.
25. Yamamoto, A., J.J. Lucas, and R. Hen, *Reversal of neuropathology and motor dysfunction in a conditional model of Huntington's disease.* Cell, 2000. **101**(1): p. 57-66.
26. Lin, F. and Z.H. Qin, *Degradation of misfolded proteins by autophagy: is it a strategy for Huntington's disease treatment?* J Huntingtons Dis, 2013. **2**(2): p. 149-57.
27. Sarkar, S., et al., *Small molecules enhance autophagy and reduce toxicity in Huntington's disease models.* Nat Chem Biol, 2007. **3**(6): p. 331-8.
28. Sasaki, T., et al., *Mammalian phosphoinositide kinases and phosphatases.* Prog Lipid Res, 2009. **48**(6): p. 307-43.
29. Rameh, L.E., et al., *A new pathway for synthesis of phosphatidylinositol-4,5-bisphosphate.* Nature, 1997. **390**(6656): p. 192-6.
30. Clarke, J.H., P.C. Emson, and R.F. Irvine, *Localization of phosphatidylinositol phosphate kinase IIgamma in kidney to a membrane trafficking compartment within specialized cells of the nephron.* Am J Physiol Renal Physiol, 2008. **295**(5): p. F1422-30.
31. Clarke, J.H., P.C. Emson, and R.F. Irvine, *Distribution and neuronal expression of phosphatidylinositol phosphate kinase IIgamma in the mouse brain.* J Comp Neurol, 2009. **517**(3): p. 296-312.
32. Lietha, D., *Phosphoinositides – The Seven Species: Conversion and Cellular Roles.* eLS, 2011.
33. Mackey, A.M., et al., *PIP4kgamma is a substrate for mTORC1 that maintains basal mTORC1 signaling during starvation.* Sci Signal, 2014. **7**(350): p. ra104.
34. Clarke, J.H., et al., *The function of phosphatidylinositol 5-phosphate 4-kinase gamma (PI5P4Kgamma) explored using a specific inhibitor that targets the PI5P-binding site.* Biochem J, 2015. **466**(2): p. 359-67.
35. Titus, S., et al., *Identification of compounds which inhibit cytotoxicity associated with mutant Huntingtin protein expression*, in *Probe Reports from the NIH Molecular Libraries Program*. 2010: Bethesda (MD).
36. Titus, S.A., et al., *High-Throughput Multiplexed Quantitation of Protein Aggregation and Cytotoxicity in a Huntington's Disease Model.* Curr Chem Genomics, 2012. **6**: p. 79-86.
37. Elrazaz, E.Z., et al., *Thieno[2,3-d]pyrimidine based derivatives as kinase inhibitors and anticancer agents.* Future Journal of Pharmaceutical Sciences, 2015. **1**(2): p. 33-41.
38. Rudolf, A.F., et al., *A comparison of protein kinases inhibitor screening methods using both enzymatic activity and binding affinity determination.* PLoS One, 2014. **9**(6): p. e98800.
39. Smyth, L.A. and I. Collins, *Measuring and interpreting the selectivity of protein kinase inhibitors.* J Chem Biol, 2009. **2**(3): p. 131-51.
40. Clarke, J.H. and R.F. Irvine, *Evolutionarily conserved structural changes in phosphatidylinositol 5-phosphate 4-kinase (PI5P4K) isoforms are responsible for differences in enzyme activity and localization.* Biochem J, 2013. **454**(1): p. 49-57.
41. Gupta, A., et al., *Phosphatidylinositol 5-phosphate 4-kinase (PIP4K) regulates TOR signaling and cell growth during Drosophila development.* Proc Natl Acad Sci U S A, 2013. **110**(15): p. 5963-8.
42. Emerling, B.S., Atsuo; Cantley, Lewis C.; Hurov, Jonathan *Modulation of phosphatidylinositol-5-phosphate-4-kinase activity*.

43. Balla, T., *Phosphoinositides: tiny lipids with giant impact on cell regulation.* Physiol Rev, 2013. **93**(3): p. 1019-137.
44. Cortes, C.J. and A.R. La Spada, *The many faces of autophagy dysfunction in Huntington's disease: from mechanism to therapy.* Drug Discov Today, 2014. **19**(7): p. 963-71.
45. Ochaba, J., et al., *Potential function for the Huntingtin protein as a scaffold for selective autophagy.* Proc Natl Acad Sci U S A, 2014. **111**(47): p. 16889-94.
46. Martin, D.D., et al., *Autophagy in Huntington disease and huntingtin in autophagy.* Trends Neurosci, 2015. **38**(1): p. 26-35.
47. Martinez-Vicente, M., et al., *Cargo recognition failure is responsible for inefficient autophagy in Huntington's disease.* Nat Neurosci, 2010. **13**(5): p. 567-76.
48. Tsvetkov, A.S., et al., *Proteostasis of polyglutamine varies among neurons and predicts neurodegeneration.* Nat Chem Biol, 2013. **9**(9): p. 586-92.
49. Roscic, A., et al., *Induction of autophagy with catalytic mTOR inhibitors reduces huntingtin aggregates in a neuronal cell model.* J Neurochem, 2011. **119**(2): p. 398-407.
50. Zhang, L., et al., *Small molecule regulators of autophagy identified by an image-based high-throughput screen.* Proc Natl Acad Sci U S A, 2007. **104**(48): p. 19023-8.
51. Renna, M., et al., *Chemical inducers of autophagy that enhance the clearance of mutant proteins in neurodegenerative diseases.* J Biol Chem, 2010. **285**(15): p. 11061-7.
52. Tanida, I., T. Ueno, and E. Kominami, *LC3 and Autophagy.* Methods Mol Biol, 2008. **445**: p. 77-88.
53. Barth, S., D. Glick, and K.F. Macleod, *Autophagy: assays and artifacts.* J Pathol, 2010. **221**(2): p. 117-24.
54. Hundeshagen, P., et al., *Concurrent detection of autolysosome formation and lysosomal degradation by flow cytometry in a high-content screen for inducers of autophagy.* BMC Biol, 2011. **9**: p. 38.
55. Kimura, S., T. Noda, and T. Yoshimori, *Dissection of the autophagosome maturation process by a novel reporter protein, tandem fluorescent-tagged LC3.* Autophagy, 2007. **3**(5): p. 452-60.
56. Mizushima, N., et al., *In vivo analysis of autophagy in response to nutrient starvation using transgenic mice expressing a fluorescent autophagosome marker.* Mol Biol Cell, 2004. **15**(3): p. 1101-11.
57. Maday, S. and E.L. Holzbaur, *Autophagosome biogenesis in primary neurons follows an ordered and spatially regulated pathway.* Dev Cell, 2014. **30**(1): p. 71-85.
58. Gupta, R., et al., *The Proline/Arginine Dipeptide from Hexanucleotide Repeat Expanded C9ORF72 Inhibits the Proteasome.* eNeuro, 2017. **4**(1).
59. Barmada, S.J., et al., *Autophagy induction enhances TDP43 turnover and survival in neuronal ALS models.* Nat Chem Biol, 2014. **10**(8): p. 677-85.
60. Kang, R., et al., *The Beclin 1 network regulates autophagy and apoptosis.* Cell Death Differ, 2011. **18**(4): p. 571-80.
61. Cui, X., et al., *TR-FRET assays of Huntingtin protein fragments reveal temperature and polyQ length-dependent conformational changes.* Sci Rep, 2014. **4**: p. 5601.
62. Shibutani, S.T. and T. Yoshimori, *A current perspective of autophagosome biogenesis.* Cell Res, 2014. **24**(1): p. 58-68.
63. Vicinanza, M., et al., *PI(5)P regulates autophagosome biogenesis.* Mol Cell, 2015. **57**(2): p. 219-34.
64. Hasegawa, J., B.S. Strunk, and L.S. Weisman, *PI5P and PI(3,5)P2: Minor, but Essential Phosphoinositides.* Cell Struct Funct, 2017. **42**(1): p. 49-60.
65. Boland, B., et al., *Autophagy induction and autophagosome clearance in neurons: relationship to autophagic pathology in Alzheimer's disease.* J Neurosci, 2008. **28**(27): p. 6926-37.

66. Munson, M.J. and I.G. Ganley, *MTOR, PIK3C3, and autophagy: Signaling the beginning from the end.* Autophagy, 2015. **11**(12): p. 2375-6.
67. Trettel, F., et al., *Dominant phenotypes produced by the HD mutation in STHdh(Q111) striatal cells.* Hum Mol Genet, 2000. **9**(19): p. 2799-809.
68. Kaltenbach, L.S., et al., *Huntingtin interacting proteins are genetic modifiers of neurodegeneration.* PLoS Genet, 2007. **3**(5): p. e82.
69. Branco, J., et al., *Comparative analysis of genetic modifiers in Drosophila points to common and distinct mechanisms of pathogenesis among polyglutamine diseases.* Hum Mol Genet, 2008. **17**(3): p. 376-90.
70. Miller, J.P., et al., *Matrix metalloproteinases are modifiers of huntingtin proteolysis and toxicity in Huntington's disease.* Neuron, 2010. **67**(2): p. 199-212.
71. Lu, B., et al., *Identification of NUB1 as a suppressor of mutant Huntington toxicity via enhanced protein clearance.* Nat Neurosci, 2013. **16**(5): p. 562-70.
72. Yao, Y., et al., *A striatal-enriched intronic GPCR modulates huntingtin levels and toxicity.* Elife, 2015. **4**.
73. Elliott, D.A. and A.H. Brand, *The GAL4 system : a versatile system for the expression of genes.* Methods Mol Biol, 2008. **420**: p. 79-95.
74. Kim, Y.E., et al., *Soluble Oligomers of PolyQ-Expanded Huntingtin Target a Multiplicity of Key Cellular Factors.* Mol Cell, 2016. **63**(6): p. 951-64.
75. Petersen, A., et al., *Expanded CAG repeats in exon 1 of the Huntington's disease gene stimulate dopamine-mediated striatal neuron autophagy and degeneration.* Hum Mol Genet, 2001. **10**(12): p. 1243-54.
76. Ravikumar, B., et al., *Inhibition of mTOR induces autophagy and reduces toxicity of polyglutamine expansions in fly and mouse models of Huntington disease.* Nat Genet, 2004. **36**(6): p. 585-95.
77. Pryor, W.M., et al., *Huntingtin promotes mTORC1 signaling in the pathogenesis of Huntington's disease.* Sci Signal, 2014. **7**(349): p. ra103.
78. Ashkenazi, A., et al., *Polyglutamine tracts regulate beclin 1-dependent autophagy.* Nature, 2017. **545**(7652): p. 108-111.
79. Caviston, J.P., et al., *Huntingtin facilitates dynein/dynactin-mediated vesicle transport.* Proc Natl Acad Sci U S A, 2007. **104**(24): p. 10045-50.
80. Wong, Y.C. and E.L. Holzbaur, *The regulation of autophagosome dynamics by huntingtin and HAP1 is disrupted by expression of mutant huntingtin, leading to defective cargo degradation.* J Neurosci, 2014. **34**(4): p. 1293-305.
81. Filimonenko, M., et al., *The selective macroautophagic degradation of aggregated proteins requires the PI3P-binding protein Alfy.* Mol Cell, 2010. **38**(2): p. 265-79.
82. Kegel, K.B., et al., *Huntingtin expression stimulates endosomal-lysosomal activity, endosome tubulation, and autophagy.* J Neurosci, 2000. **20**(19): p. 7268-78.
83. Duan, W., et al., *Dietary restriction normalizes glucose metabolism and BDNF levels, slows disease progression, and increases survival in huntingtin mutant mice.* Proc Natl Acad Sci U S A, 2003. **100**(5): p. 2911-6.
84. Ikenaka, K., et al., *dnc-1/dynactin 1 knockdown disrupts transport of autophagosomes and induces motor neuron degeneration.* PLoS One, 2013. **8**(2): p. e54511.
85. Shim, H., et al., *Deletion of the gene Pip4k2c, a novel phosphatidylinositol kinase, results in hyperactivation of the immune system.* Proc Natl Acad Sci U S A, 2016. **113**(27): p. 7596-601.
86. Zolov, S.N., et al., *In vivo, Pikfyve generates PI(3,5)P2, which serves as both a signaling lipid and the major precursor for PI5P.* Proc Natl Acad Sci U S A, 2012. **109**(43): p. 17472-7.

87. McCartney, A.J., et al., *Activity-dependent PI(3,5)P2 synthesis controls AMPA receptor trafficking during synaptic depression.* Proc Natl Acad Sci U S A, 2014. **111**(45): p. E4896-905.
88. Sbrissa, D., et al., *Functional dissociation between PIKfyve-synthesized PtdIns5P and PtdIns(3,5)P2 by means of the PIKfyve inhibitor YM201636.* Am J Physiol Cell Physiol, 2012. **303**(4): p. C436-46.
89. Carlsson, S.R. and A. Simonsen, *Membrane dynamics in autophagosome biogenesis.* J Cell Sci, 2015. **128**(2): p. 193-205.
90. Ikonomov, O.C., D. Sbrissa, and A. Shisheva, *Localized PtdIns 3,5-P2 synthesis to regulate early endosome dynamics and fusion.* Am J Physiol Cell Physiol, 2006. **291**(2): p. C393-404.
91. Rong, Y., et al., *Clathrin and phosphatidylinositol-4,5-bisphosphate regulate autophagic lysosome reformation.* Nat Cell Biol, 2012. **14**(9): p. 924-34.
92. Yu, L., et al., *Termination of autophagy and reformation of lysosomes regulated by mTOR.* Nature, 2010. **465**(7300): p. 942-6.
93. de Lartigue, J., et al., *PIKfyve regulation of endosome-linked pathways.* Traffic, 2009. **10**(7): p. 883-93.
94. Jin, N., et al., *VAC14 nucleates a protein complex essential for the acute interconversion of PI3P and PI(3,5)P(2) in yeast and mouse.* EMBO J, 2008. **27**(24): p. 3221-34.
95. Jin, N., et al., *Roles for PI(3,5)P2 in nutrient sensing through TORC1.* Mol Biol Cell, 2014. **25**(7): p. 1171-85.
96. Ikonomov, O.C., D. Sbrissa, and A. Shisheva, *Mammalian cell morphology and endocytic membrane homeostasis require enzymatically active phosphoinositide 5-kinase PIKfyve.* J Biol Chem, 2001. **276**(28): p. 26141-7.
97. Martin, S., et al., *Inhibition of PIKfyve by YM-201636 dysregulates autophagy and leads to apoptosis-independent neuronal cell death.* PLoS One, 2013. **8**(3): p. e60152.
98. Rusten, T.E., et al., *ESCRTs and Fab1 regulate distinct steps of autophagy.* Curr Biol, 2007. **17**(20): p. 1817-25.
99. Sano, O., et al., *Vacuolin-1 inhibits autophagy by impairing lysosomal maturation via PIKfyve inhibition.* FEBS Lett, 2016. **590**(11): p. 1576-85.
100. Burke, K.A., et al., *Huntingtin disrupts lipid bilayers in a polyQ-length dependent manner.* Biochim Biophys Acta, 2013. **1828**(8): p. 1953-61.
101. Kegel, K.B., et al., *Polyglutamine expansion in huntingtin increases its insertion into lipid bilayers.* Biochem Biophys Res Commun, 2009. **387**(3): p. 472-5.
102. Kegel, K.B., et al., *Polyglutamine expansion in huntingtin alters its interaction with phospholipids.* J Neurochem, 2009. **110**(5): p. 1585-97.
103. Kegel, K.B., et al., *Huntingtin associates with acidic phospholipids at the plasma membrane.* J Biol Chem, 2005. **280**(43): p. 36464-73.
104. Kegel-Gleason, K.B., *Huntingtin interactions with membrane phospholipids: strategic targets for therapeutic intervention?* J Huntingtons Dis, 2013. **2**(3): p. 239-50.
105. Komatsu, M., et al., *Constitutive autophagy: vital role in clearance of unfavorable proteins in neurons.* Cell Death Differ, 2007. **14**(5): p. 887-94.
106. Igwe, O.J. and M.B. Filla, *Regulation of phosphatidylinositide transduction system in the rat spinal cord during aging.* Neuroscience, 1995. **69**(4): p. 1239-51.
107. Speakman, J.R. and C. Hambly, *Starving for life: what animal studies can and cannot tell us about the use of caloric restriction to prolong human lifespan.* J Nutr, 2007. **137**(4): p. 1078-86.
108. Hara, T., et al., *Suppression of basal autophagy in neural cells causes neurodegenerative disease in mice.* Nature, 2006. **441**(7095): p. 885-9.
109. Seino, J., et al., *Basal autophagy is required for the efficient catabolism of sialyloligosaccharides.* J Biol Chem, 2013. **288**(37): p. 26898-907.

110. Wang, M., et al., *Genomic tagging reveals a random association of endogenous PtdIns5P 4-kinases IIalpha and IIbeta and a partial nuclear localization of the IIalpha isoform.* Biochem J, 2010. **430**(2): p. 215-21.
111. Clarke, J.H., et al., *Inositol lipids are regulated during cell cycle progression in the nuclei of murine erythroleukaemia cells.* Biochem J, 2001. **357**(Pt 3): p. 905-10.
112. Bligh, E.G. and W.J. Dyer, *A rapid method of total lipid extraction and purification.* Can J Biochem Physiol, 1959. **37**(8): p. 911-7.
113. Narain, Y., et al., *A molecular investigation of true dominance in Huntington's disease.* J Med Genet, 1999. **36**(10): p. 739-46.
114. Komatsu, M., et al., *Impairment of starvation-induced and constitutive autophagy in Atg7-deficient mice.* J Cell Biol, 2005. **169**(3): p. 425-34.
115. Saudou, F., et al., *Huntingtin acts in the nucleus to induce apoptosis but death does not correlate with the formation of intranuclear inclusions.* Cell, 1998. **95**(1): p. 55-66.
116. Barmada, S.J., et al., *Amelioration of toxicity in neuronal models of amyotrophic lateral sclerosis by hUPF1.* Proc Natl Acad Sci U S A, 2015. **112**(25): p. 7821-6.
117. El-Daher, M.T., et al., *Huntingtin proteolysis releases non-polyQ fragments that cause toxicity through dynamin 1 dysregulation.* EMBO J, 2015. **34**(17): p. 2255-71.

Figure legends

Figure 1. Identification of NCT-504 and its inhibition of PIP4Kγ. A) Structure of NCT-504. **B)** NCT-504 treatment reduces Htt(exon1)-Q103 in PC12 cells. Cells with stable expression of ecdysone-inducible GFP-Htt(exon1)-Q103 (green), induced for 24 hr, and treated with DMSO (top panels) or 23 μM NCT-504 (bottom). Cells stained with DAPI (blue). Scale Bar = 50 μm. **C)** Concentration-response curve of NCT-504 inhibition of cellular accumulation of GFP-Htt(exon1)-Q103. **D)** NCT-504 inhibition of PIP4Kγ binding to an immobilized proprietary active site ligand DiscoverX KINOME*scan*® https://www.discoverx.com/services/drug-discovery-development-services/kinase-profiling/kinomescan). **E)** NCT-504 exhibits dose-dependent inhibition of phosphorylation of PI4P by full length isolated PIP4Kγ. **F)** The intrinsic ATPase specific activity of full length isolated PIP4Kγ in the absence of PI5P substrate as a function of NCT-504 concentration is the same in the presence (blue) or in the absence (purple) of NCT-504.

Figure 2. Pharmacologic and genetic inhibition of PIP4Kγ elevates the levels of PI(3,5)P2, PI3P and PI5P in MEFs. A-F) Pharmacologic (NCT-504 10 μM, 12 hours) and genetic (shRNA) inhibition of PIP4Kγ leads to increased levels of PI5P (**D**), PI(3,5)P2 (**E**) and PI3P (**B**), with no significant change in the levels of phosphatidylinositol (**A**), PI4P (**C**) or PI(4,5)P2 (**F**). However, there was a modest reduction in PI4P. Note in Figure 2 – figure supplement 2, this small change was statically significant. Measurements were performed in MEF cells incubated with ^{3}H-inositol labeled media for 48 hours. Statistical significance was analyzed using paired one tailed student t-test (n=3), * $p<0.05$, ** $p<0.01$. **G**) Anti-PIP4Kγ western blot showing the effective silencing of the enzyme using shRNA. (GAPDH used as loading control)

Figure 3. Inhibition of PIP4Kγ increases autophagy flux. A) Representative Western blots showing the levels of LC3-I, LC3-II and Tubulin (loading control) in HEK293T cells treated with either 5 or 10 μM NCT-504 or DMSO (control) for two or six hours in the presence or absence of 100 nM bafilomycin. **B-C**) Quantification of LC3-II levels detected by western blot normalized to α-tubulin (loading control). Changes in LC3-II with drug treatment alone is presented relative to levels in the DMSO control cell lysates (B) and changes in LC3-II with drug treatment plus bafilomycin is presented relative to DMSO plus bafilomycin (C). Statistical significance was quantified from three independent experiments using Dunnett's multiple comparisons test, * $p<0.05$, ** $p<0.01$, *** $p<0.005$.

Figure 4. Chemical inhibition of PIP4Kγ or knock-down of the corresponding mRNA, PIP4K2C, lowers mHtt protein levels in cells from HD patients and HD knock-in mice. A) Reduction of mHtt protein levels in an HD patient fibroblast cell line (Q68) following exposure for 12 hours to NCT-504 (5 μM) **B)** mHtt protein levels in patient fibroblast cell line (Q68) were analyzed following siRNA-mediated silencing of PIP4K2A, PIP4K2B and PIP4K2C genes. Note that only PIP4K2C knockdown lowers mHtt levels. Control experiments showing silencing specificity on PIP4K protein levels are in Figure 4 – figure supplement 3. **C)** Reduction of mHtt protein levels in an HD patient fibroblast cell line (Q45) following exposure to NCT-504 (5 μM). **D)** Reduction of mHtt protein levels in immortalized striatal cells from knock-in HD mice (ST*Hdh*Q111) treated for 12 hours with NCT-504 (5 μM).

Figure 5. Reduced dPIP4K gene activity ameliorates photoreceptor degeneration and behavioral impairments in a Drosophila HD model. A) Sections through the *Drosophila* retina showing loss of photoreceptor cells and retinal tissue in animals expressing N-terminal mHtt (HTTNT231Q128) in the eye (compare no modifier with negative control panels). The photoreceptor and retinal loss phenotype is ameliorated in HttNT231Q128 animals that also express anyone of two shRNAs targeting dPIP4K. **B**) Chart shows motor performance (%) as a function of age in negative controls (dPIP4K+/+, blue dotted line), *Drosophila* expressing N-terminal mHtt in the CNS (HTTNT231Q128/ dPIP4K+/+, black line) or animals expressing N-terminal mHtt in the CNS together with a dPIP4K heterozygous loss of function (HTTNT231Q128/ dPIP4K+/-, red continuous line) or a dPIP4K kinase dead isoform (HTTNT231Q128/ dPIP4K+/DN, green continuous line). Notice the amelioration of mHtt-induced deficits upon decreasing the activity of dPIP4K. **C**) Chart shows motor performance (%) and climbing speed as a function of age in negative controls (dPIP4K+/+, blue dotted line), *Drosophila* expressing full length mHtt in the CNS (HTT-FLQ200/ dPIP4K+/+, black line) or animals expressing FL mHtt in the CNS together with a dPIP4K heterozygous loss of function (HTT-FL200 / dPIP4K+/-, red continuous line) or a dPIP4K kinase dead isoform (HTT-FL200 / dPIP4K+/DN, green continuous line). Note amelioration of neural HttNT231Q128-induced motor deficits by decreasing the activity of dPIP4K. Genotypes in A: Negative control: *GMR-GAL4/+; dPIP4K+/+* . No modifier: *GMR-GAL4/+; UAS:HTTNT231Q128/+; dPIP4K+/+*. PIP4K2 sh1/sh2: *GMR-GAL4/+; UAS:HTTNT231Q128/UAS:dPIP4Ksh-1 or sh-2* . Genotypes in B: Negative control: *elavc155GAL4/+; dPIP4K+/+*.HTT231Q128: *elavc155GAL4/+; UAS:HttNT231Q128/+; dPIP4K+/+* . HTT231Q128 /PIP4K2^{LOF}: *elavc155GAL4/+; UAS:HttNT231Q128/+; dPIP4K29/+* and HTT231Q128 /PIP4K2^{DN}: *elavc155GAL4/+; UAS:HttNT231Q128/UAS:dPIP4K29[D271K]*. . Genotypes in C: Negative control: *elavc155GAL4/+; dPIP4K+/+*. HTT-FLQ200: *elavc155GAL4/+; UAS:HttFLQ200/+; dPIP4K+/+* . HTT-FLQ200 /PIP4K2^{LOF} : *elavc155GAL4/+; UAS:UAS:HttFLQ200/+; dPIP4K29/+* and HTT-FLQ200 /PIP4K2^{DN} : *elavc155GAL4/+; UAS:UAS:HttFLQ200/UAS:dPIP4K29[D271K]* . elavc155GAL4 drives expression of mHtt to all neurons but not other cell types. Means between points at each age were analyzed by ANOVA followed by Dunnet's post hoc test. Error bars indicate the s.e.m. *=$p<0.05$.

Supplementary figure legends

Figure 1 – figure supplement 1. NCT-504 suppresses the accumulation of HTT-exon1 aggregates. HEK293T cells were either transfected with GFP-HTT(exon1)-Q23 or GFP-HTT(exon1)-Q74. Two hours after transfection, cells were either treated with DMSO or NCT-504 (2 μM). After 48 hour of treatment, cells were fixed and quantified for the percentage of cells with aggregates. Results from three independent experiments. Statistical significance was analyzed using paired one tailed student T test *** $p<0.005$. Bar = 50 μm.

Figure 1 – figure supplement 2. NCT-504 does not inhibit PIP4Kbeta and weakly inhibits PIP4Kalpha phosphorylation of PI5P. Results from three independent experiments are shown

for inhibition of phosphorylation of PI5P. **A)** PIP4Kalpha with 50 μM NCT-504, **B)** 100 μM NCT-504, and **C)** PIP4Kbeta with 100 μM NCT-504

Figure 1 – figure supplement 3. A PIP4Kγ+ G-loop mutant is resistant to inhibition by NCT-504, consistent with NCT-504 functioning as an allosteric inhibitor. PIP4Kγ+ contains mutations in the G-loop and additional mutations that increase the low intrinsic ATP turnover exhibited by PIP4Kγ in the presence of PI5P. The PIP4Kγ+ mutant kinase is described as PI5P4Kγ G3A+B in reference [40]. NCT-504 was almost inactive (potency >500μM) against PIP4Kγ+ (blue). In comparison, activity against the PIP4Kγ construct at DiscoverRx KINOME*scan*® assay) results are shown in black. N=3 for each concentration tested. The data is presented as % inhibition of kinase binding to a proprietary active site immobilized ligand by a compound that binds to the kinase active site directly (sterically) or indirectly (allosterically). (https://www.discoverx.com/technologies-platforms/competitive-binding-technology/kinomescan-technology-platform)

Figure 2 – figure supplement 1. NCT-504 treatment does not affect cell viability in MEFs. Primary MEF cells treated with 10 μM NCT-504 or DMSO (control) for 12 hours were incubated with Hoechst 33342 and ethidium homodimer (Ethd1) for 15 min to measure cell viability. Ethd1 is impermeable to the nucleus in live cells; whereas in dead cells, Ethd1 displaces Hoechst and stains the nucleus red. Percentage of cells negative for Ethd1-nuclear stain were quantified from three experiments. A minimum of 640 cells were analyzed. White arrow indicates a dead cell. Scale Bar 100 μm. Student's one-tailed t-test indicates no statistically significant difference between DMSO and NCT-504 treatment.

Figure 2 – figure supplement 2. **Time course of phosphatidylinositol lipid changes upon NCT-504 treatment (10 μM) in MEFs.** Time shown in minutes: 0, 5, 30, 120, 720 min. Average of three experiments with error bars. Statistical significance between DMSO-treated and NCT-504 treated samples were analyzed using paired one tailed student t-test, * $p<0.05$, ** $p<0.01$, *** $p<0.005$, **** $p<0.001$, ***** $p<0.0005$.

Figure 2 – figure supplement 3. Modulation of the levels of phosphatidylinositol lipids by NCT-504 in unaffected human fibroblasts. Immortalized human fibroblast cells were incubated with media containing ^{3}H-inositol for 48 hours and cells were treated with DMSO or indicated concentrations of NCT-504 for the last 12 hours of labeling.

Figure 3 – figure supplement 1. NCT-504 increases autophagy flux and decreases huntingtin protein in 293A cells. Concentration-response of bafilomycin (20nM, 40nM, 80nM, 160nM, 320nM), torin-1 (20nM, 40nM, 80nM, 160nM, 320nM), and NCT-504 (2.4μM, 4.8μM, 10μM, 20μM, 40μM) as modulators of autophagosome formation and autophagy flux. **A)** Autophagosome formation was measured, at 11 hours, as increase of total yellow spots area (GFP spots area overlap with mCherry spots area) normalized with DMSO treatment control from an image taken at each time point using the Opera Phenix™ (PerkinElmer), data presented here is average of N=3, one field per well, **B)** Autophagy flux at 11 hours was monitored via autolysosome formation as measured by the increase of total red spots area

(mCherry spots area) normalized with DMSO treatment control, data presented here is average of N=3, one field per well, **C)** Change in huntingtin protein measured by Homogeneous Time Resolved Fluorescence (HTRF®) assay at 48 hours, and **D)** change in viability of cells following treatment as measured by ATP concentration using CellTiter-Glo® Luminescent Cell Viability Assay (Promega).

Figure 3 – figure supplement 2. PIP4Kγ inhibition increases the rate of autophagic flux in cortical neurons. The effect of NCT-504 on autophagic flux was determined in DIV4 rat primary cortical neurons transfected with Dendra2-LC3. Untreated (UT) and DMSO-treated neurons are negative controls; co-transfection with GFP-Beclin serves as a positive control. 30 min post-transfection, neurons were treated with DMSO or NCT-504. After 24 hours, Dendra2-LC3 was photoconverted and the intensity of red Dendra2-LC3 within each neuron was quantified immediately and at 4 additional time points for a duration of 2 days. A minimum of 750 neurons were quantified for each condition with the exception of 540 for Beclin-transfected neurons. Dendra2-LC3 half-life was calculated from the rate of loss of red-Denra2-LC3 intensity. Kruskal-Wallis ($c2$ (5, n= 4,743) =177.4, $P<0.0001$) and Dunnet's post hoc test results indicate that differences between no treatment and each treatment are significant: Beclin ($P<0.0001$), 0.5 µM NCT-504 ($P<0.0001$) and 1 µM NCT-504 ($P=0.0003$). *= $P<0.0005$.

Figure 3 – figure supplement 3. Lowering mHtt aggregates via NCT-504 requires macroautophagy: A-B) *Atg7+/+* and *Atg7-/-* cells were transfected with GFP-Htt(exon1)-Q74. Two hours after transfection, cells were treated with either DMSO or 2 µM NCT-504 for 48 hours, fixed, and the percentage of cells with aggregates was quantified. The ratio of aggregates in NCT-504 vs. DMSO treatments were determined separately for wild-type and mutant cells. Statistical significance was analyzed using paired one tailed student t-test from three individual experiments. **$P<0.01$, *$P<0.05$. Bar 20 µm. **C)** *Atg7+/+* and *Atg7-/-* cells were lysed and immunoblotted with antibodies against Atg7 and GADPH.

Figure 4 – figure supplement 1. Cell viability of HD patient fibroblasts (Q45) exposed to the indicated doses of NCT-504 for 12 hours CellTiter-Glo Promega assay.

Figure 4 – figure supplement 2. Knock-down efficiency and specificity of small interfering RNA in HD patient fibroblasts (Q45). Cells grown in 35 mm culture dishes were treated with 800 pmoles of On-target plus smartpool SiRNA for 72 hours. Cells were lysed and immunoblotted with antibodies for PIP4Kα, PIP4Kβ, PIP4Kγ and GADPH.

Figure 4 – figure supplement 3. Experimental details and controls for mouse primary cortical neurons transduced with Htt(exon1)-Q72. A) Experimental design of PIP4Kγ inhibitor treatment in neurons. Mouse primary cortical neurons transduced with Htt(exon1)-Q72 lentivirus and treated with PIP4Kγ inhibitor NCT-504 for 48 hrs. **B)** Assessment of baseline toxicity of NCT-504 to find non-toxic concentrations. The indicated concentrations of NCT-504 were applied to neurons for 48 hrs and baseline toxicity assessed by in-cell western analysis using neurofilament antibody. To normalize cell number Draq5 and sapphire 700 staining (D+S) was performed. Veh represents vehicle (DMSO) treatment.

Figure 4 – figure supplement 4. Reduction of Htt protein levels or aggregate by inhibition of PIP4Kγ or PIP4K2C knockdown. A) NCT-504 reduces the levels of Htt(exon1)-Q72 in primary cortical mouse neurons as measured by western blot analysis using the monoclonal antibody 5TF-1C2, which recognizes polyQ. β-tubulin was used as a loading control. **B)** Effect of knockdown of PIP4K2C on mHtt aggregates in mouse primary cortical neurons, as measured by two-dimensional resolution of high molecular weight species using AGERA.

Figure 4 – figure supplement 5. Effect of PIP4K2C knockdown on mHtt aggregates in N2a transfected cells. A) Effect of knockdown on PIP4Kγ protein assessed by western of N2a cell lysates. This is a Neuro-2a neuroblastoma cell line purchased from the ATCC (RRID: CVCL_0470) **B)** Effect of knockdown of PIP4K2C on formation of mHtt aggregates as measured by two-dimensional resolution of high molecular weight species using AGERA. Htt(exon1) polyglutamine expansion lengths are indicated.

Figure 5 – figure supplement 1. Reduced dPIP4K gene activity in wild type Drosophila does not impact motility.

Table 1

Kinase	ML168	NCT-504
PIP4K2C	23	4.9
RSK1(Kin.Dom.2-C-terminal)	20	40
GAK	10	42

% Control Legend	0%≤x<10%	10%≤x<35%	35%≤x

Table 1. **Kinase profiling results for NCT-504 and ML168.** Percent activity remaining at 10 μM exposure of NCT-504 and ML168 in KINOMEscan kinase panel/profiling http://www.discoverx.com/technologies-platforms/competitive-binding-technology/kinomescan-technology-platform. Top 3 NCT-504 inhibited kinases are reported as single replicate data. Full data set is provided in Table 1 – source data file. PIP4K2γ potencies were confirmed in triplicate concentration-response testing (Figure 1D).

Source Code file 1. Custom Software for statistical analysis.

Figure 1

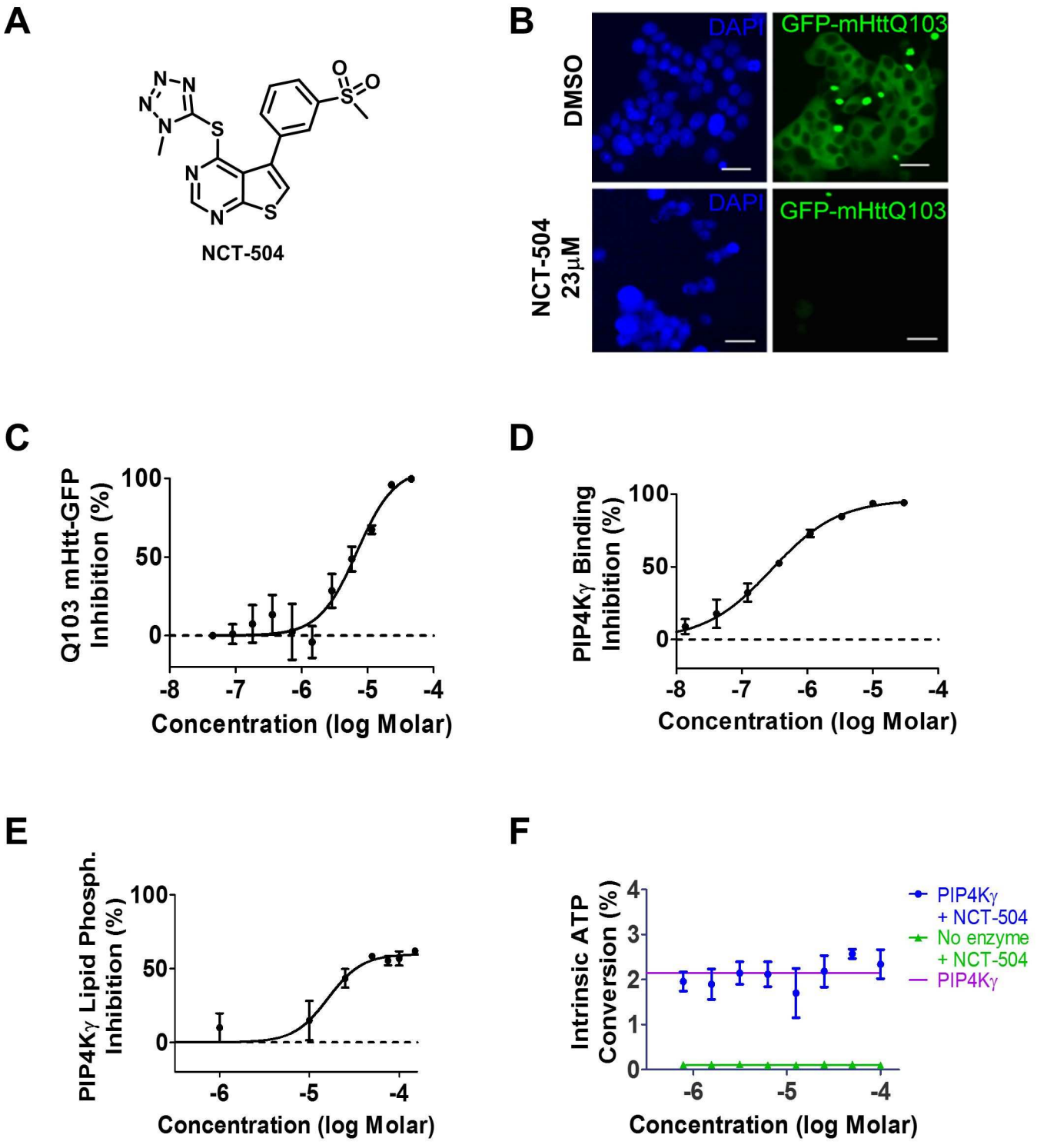
A
NCT-504
B
DAPI
GFP-mHttQ103
DMSO
NCT-504
23μM
C
Q103 mHtt-GFP
Inhibition (%)
Concentration (log Molar)
D
PIP4Kγ Binding
Inhibition (%)
Concentration (log Molar)
E
PIP4Kγ Lipid Phosph.
Inhibition (%)
Concentration (log Molar)
F
Intrinsic ATP
Conversion (%)
PIP4Kγ
+ NCT-504
No enzyme
+ NCT-504
PIP4Kγ
Concentration (log Molar)

Figure 1 – figure supplement 1

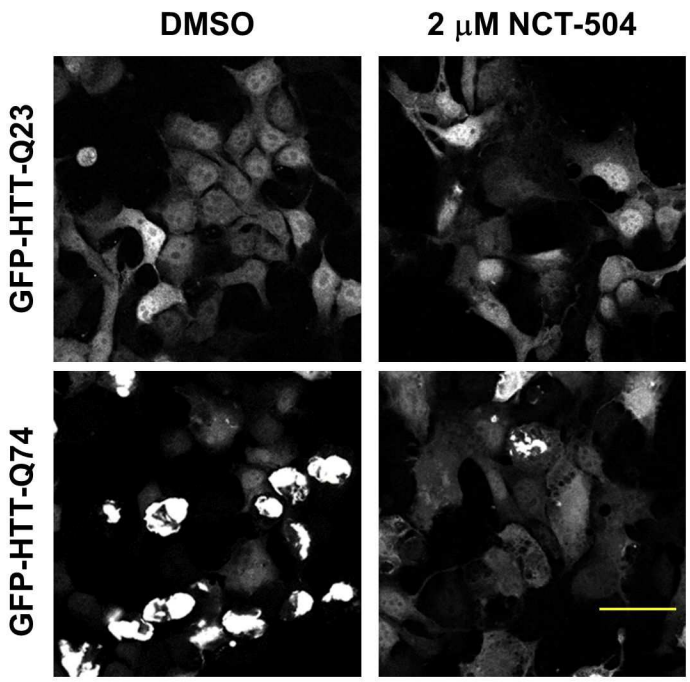

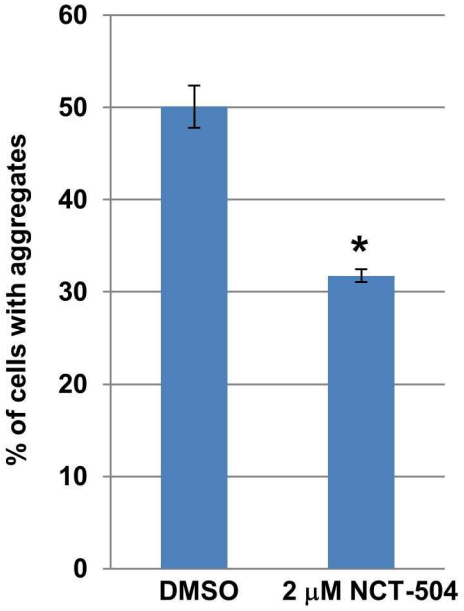

Figure 1 – figure supplement 2

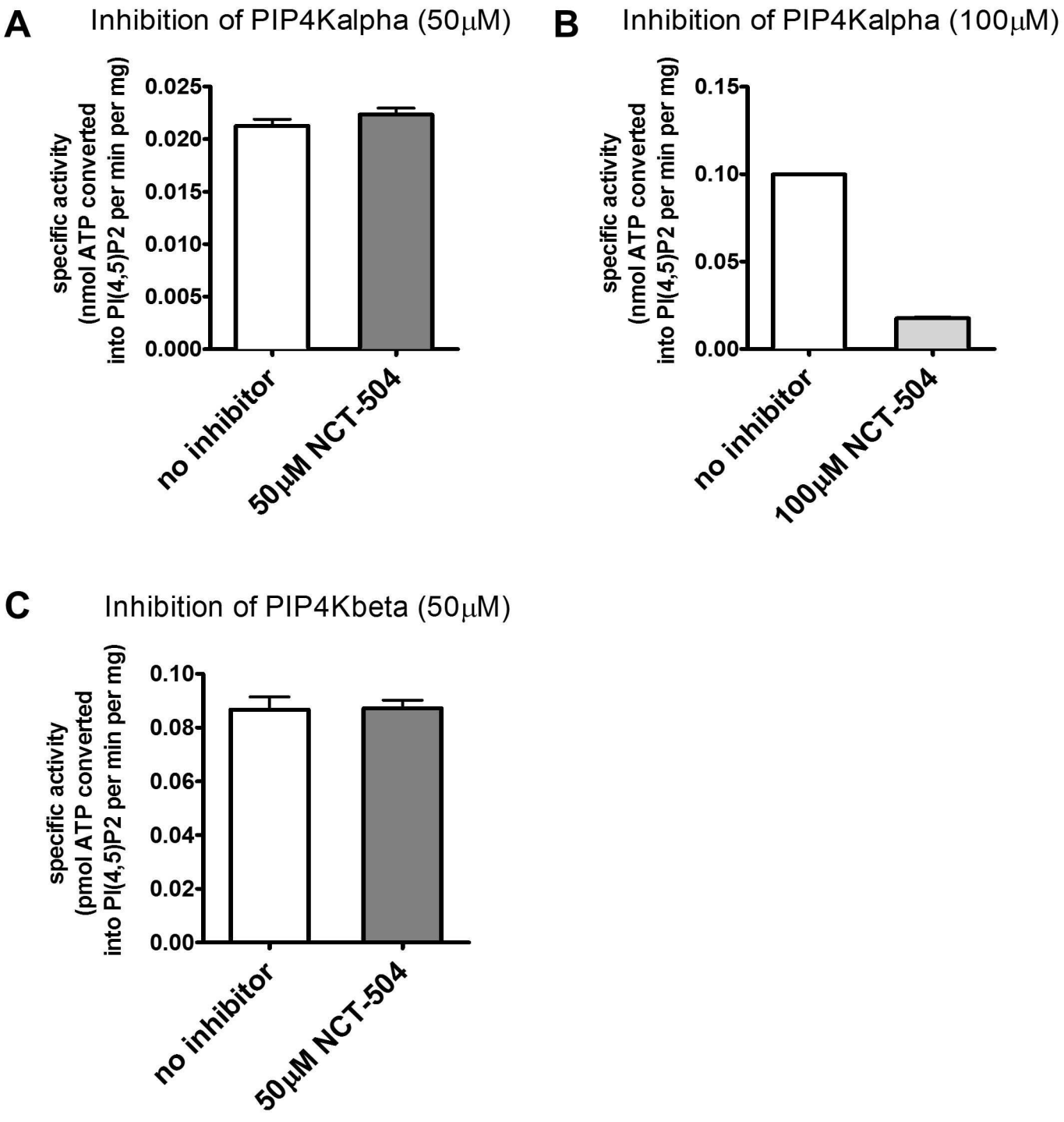

Figure 1 – figure supplement 3

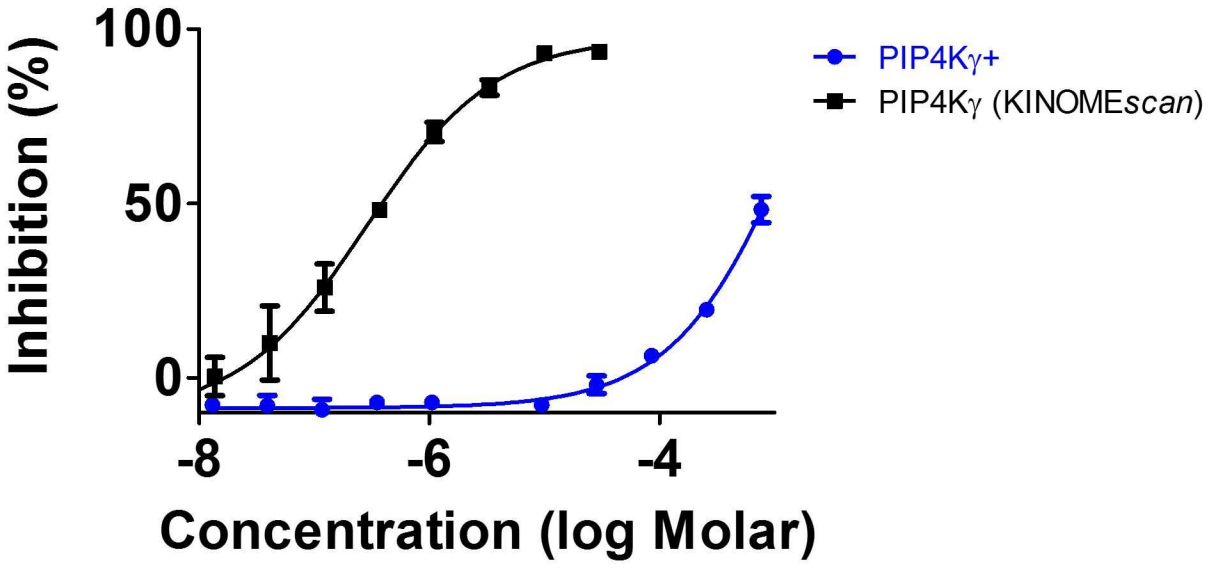

Figure 2

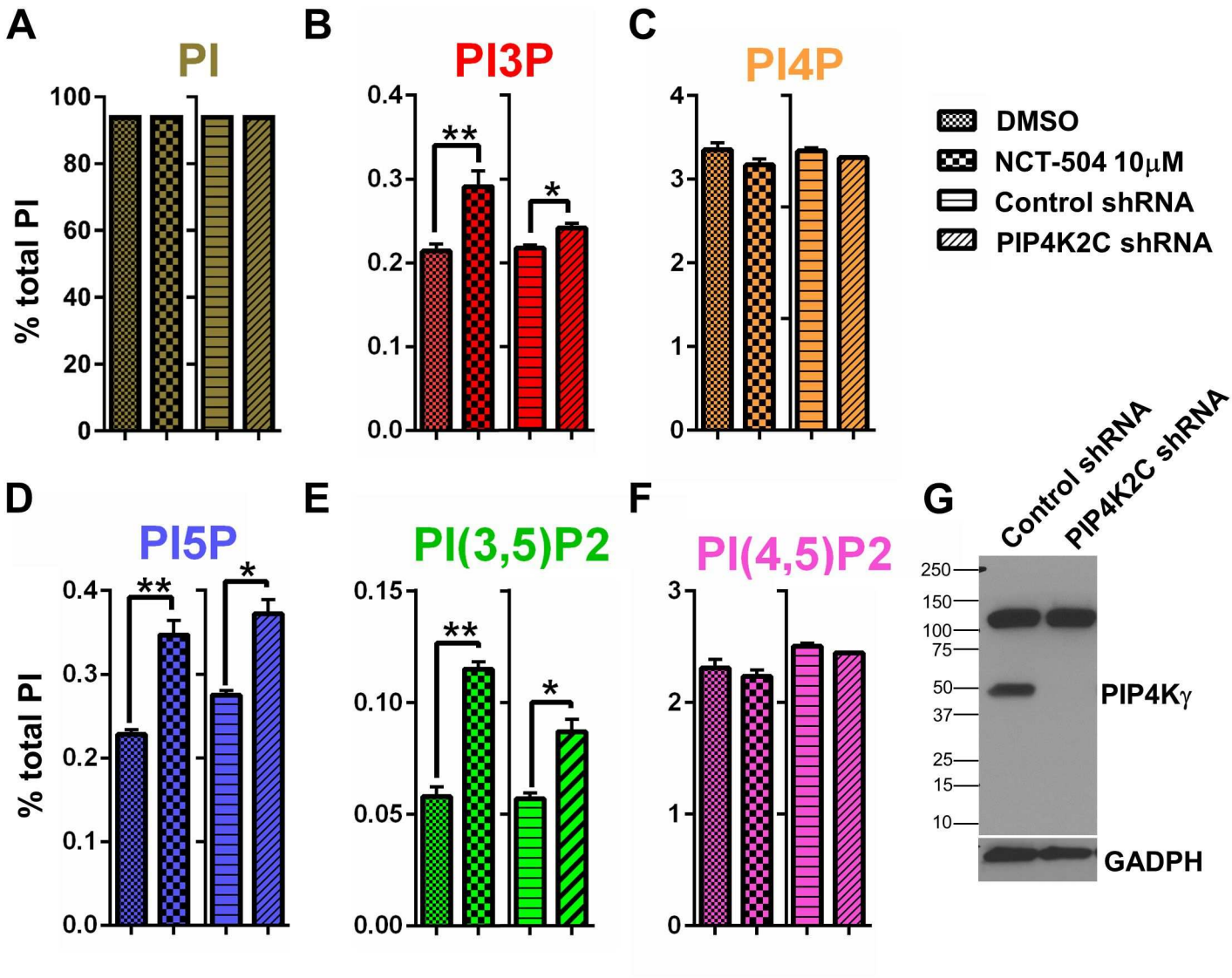
A
PI
% total PI
100
80
60
40
20
0
B
PI3P
0.4
0.3
0.2
0.1
0.0
**
*
C
PI4P
4
3
2
1
0
DMSO
NCT-504 10μM
Control shRNA
PIP4K2C shRNA
D
PI5P
% total PI
0.4
0.3
0.2
0.1
0.0
**
*
E
PI(3,5)P2
0.15
0.10
0.05
0.00
**
*
F
PI(4,5)P2
3
2
1
0
G
Control shRNA
PIP4K2C shRNA
250
150
100
75
50
37
25
15
10
PIP4Kγ
GADPH

Figure 2 – figure supplement 1

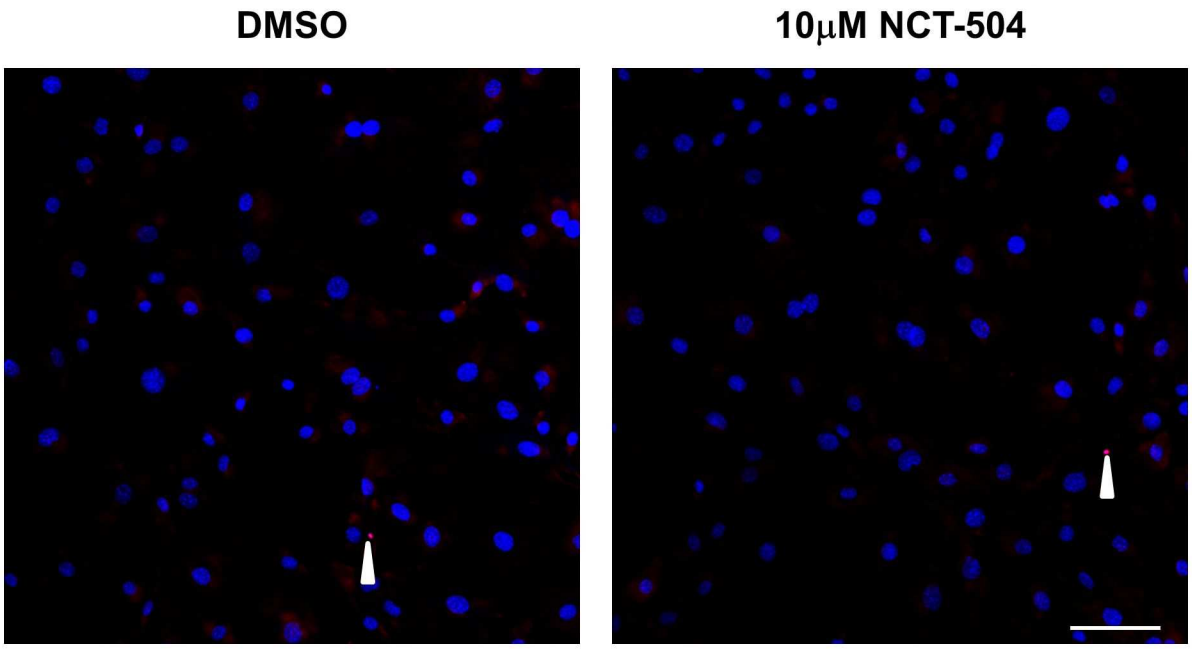

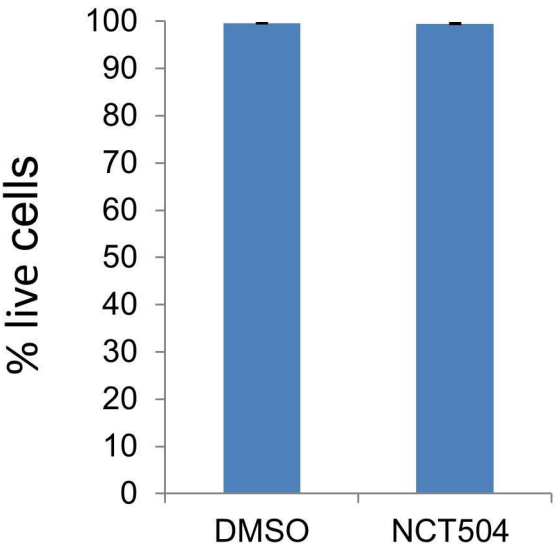

Figure 2 – figure supplement 2

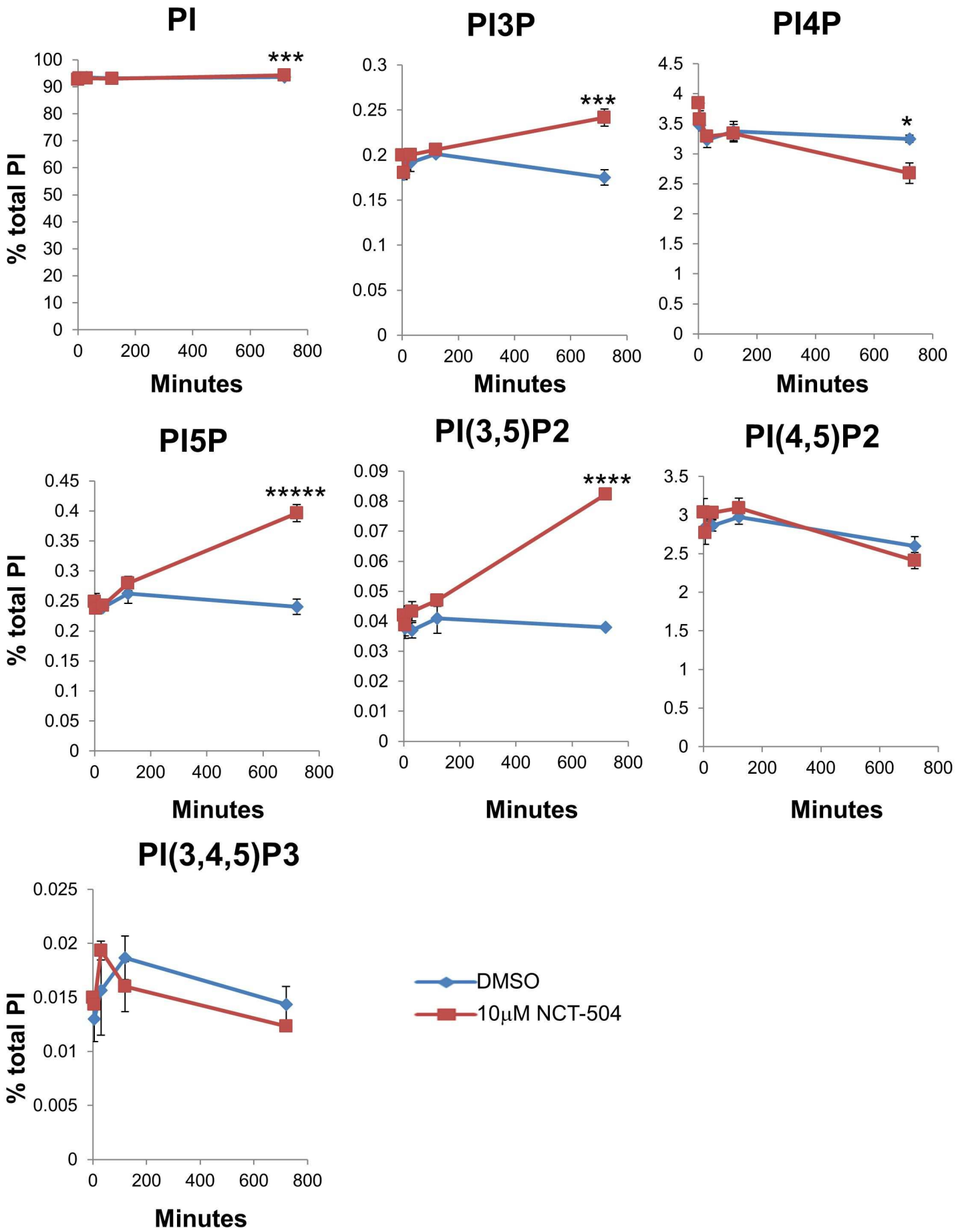

Figure 2 – figure supplement 3

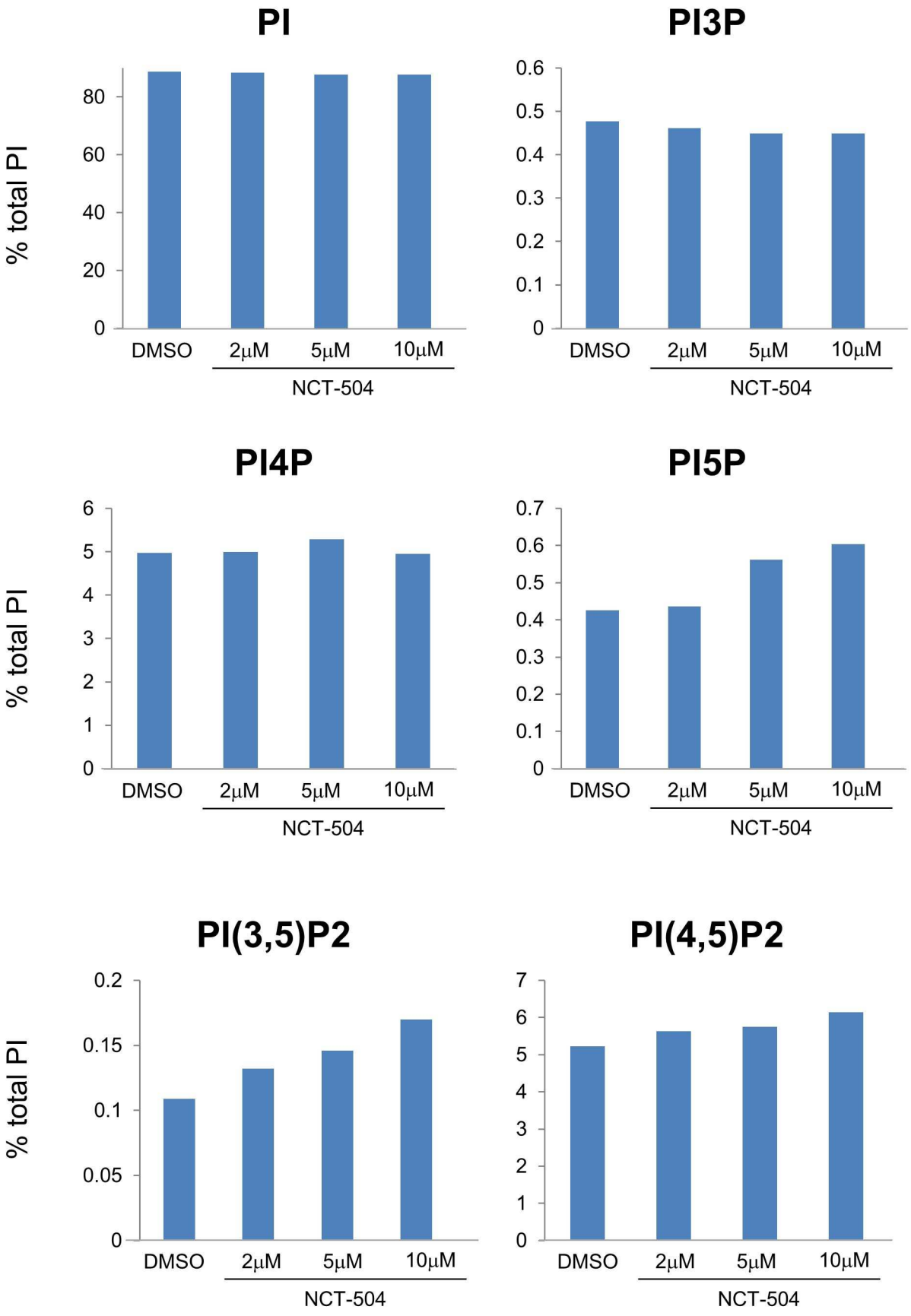

Figure 3

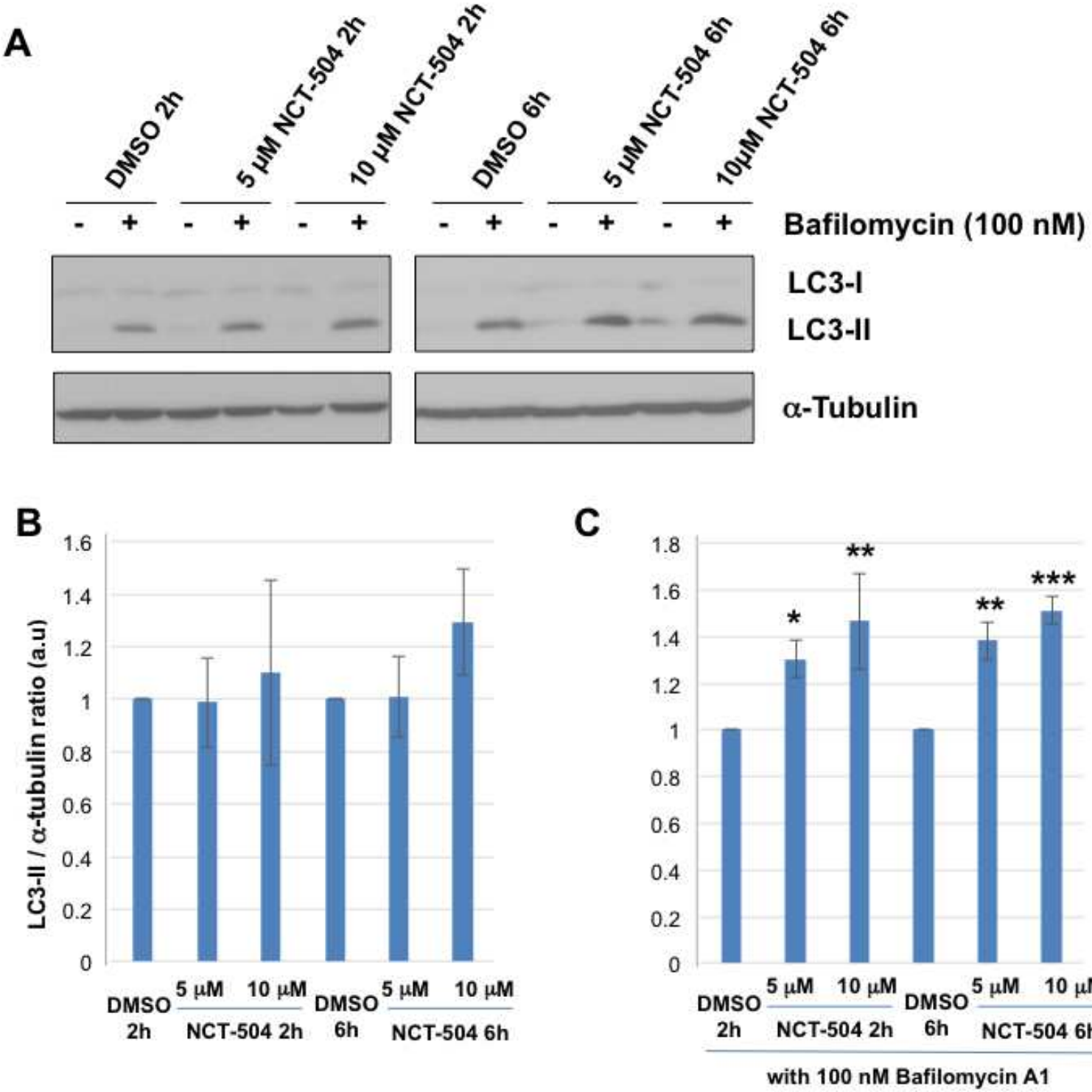
A
DMSO 2h
5 μM NCT-504 2h
10 μM NCT-504 2h
DMSO 6h
5 μM NCT-504 6h
10μM NCT-504 6h
- + - + - + - + - + - +
Bafilomycin (100 nM)
LC3-I
LC3-II
α-Tubulin
B
LC3-II / α-tubulin ratio (a.u)
1.6
1.4
1.2
1
0.8
0.6
0.4
0.2
0
DMSO 2h
5 μM
10 μM
NCT-504 2h
DMSO 6h
5 μM
10 μM
NCT-504 6h
C
1.8
1.6
1.4
1.2
1
0.8
0.6
0.4
0.2
0
*
**
**
***
DMSO 2h
5 μM
10 μM
NCT-504 2h
DMSO 6h
5 μM
10 μM
NCT-504 6h
with 100 nM Bafilomycin A1

Figure 3 – figure supplement 1

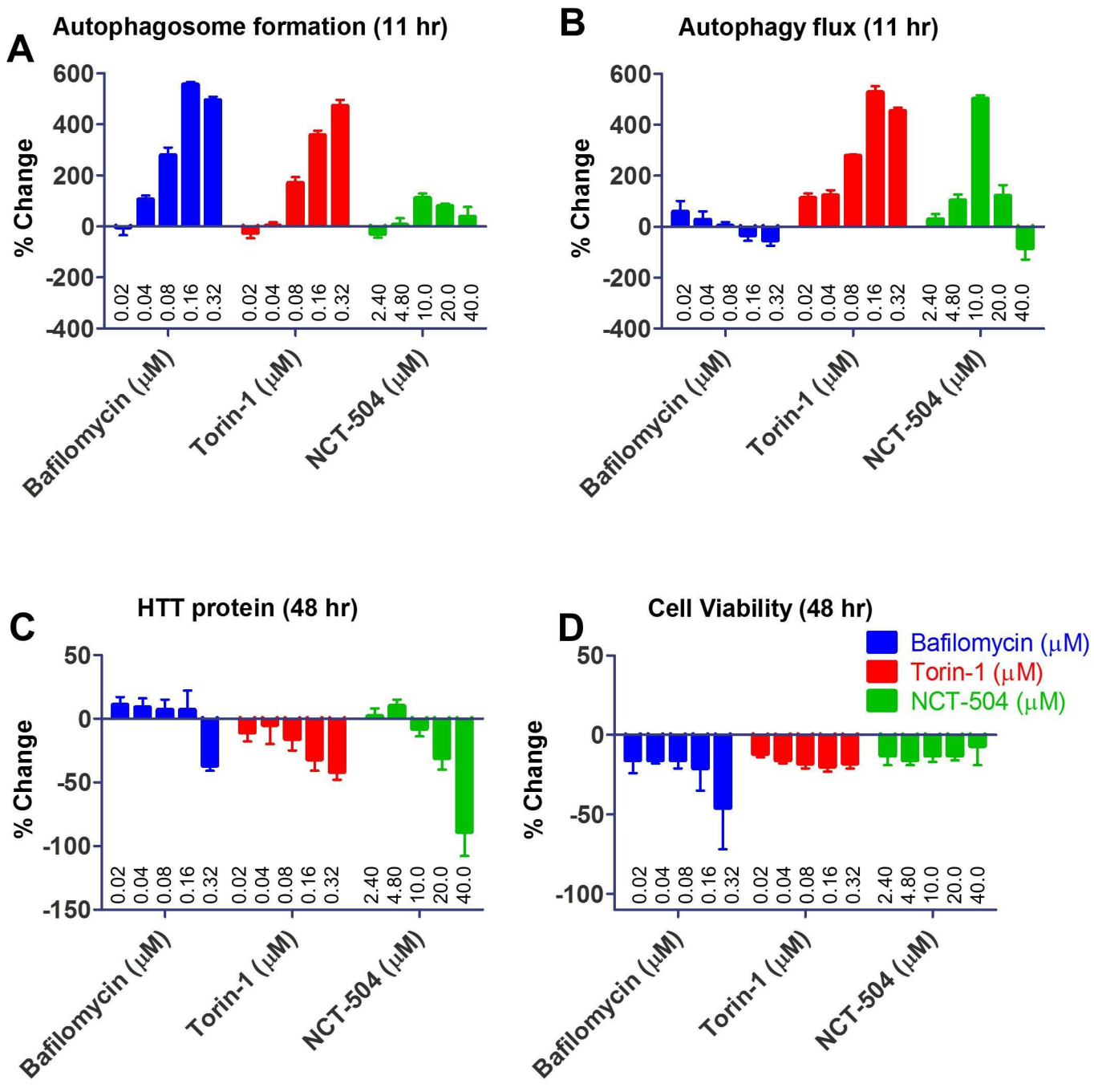

Figure 3 – figure supplement 2

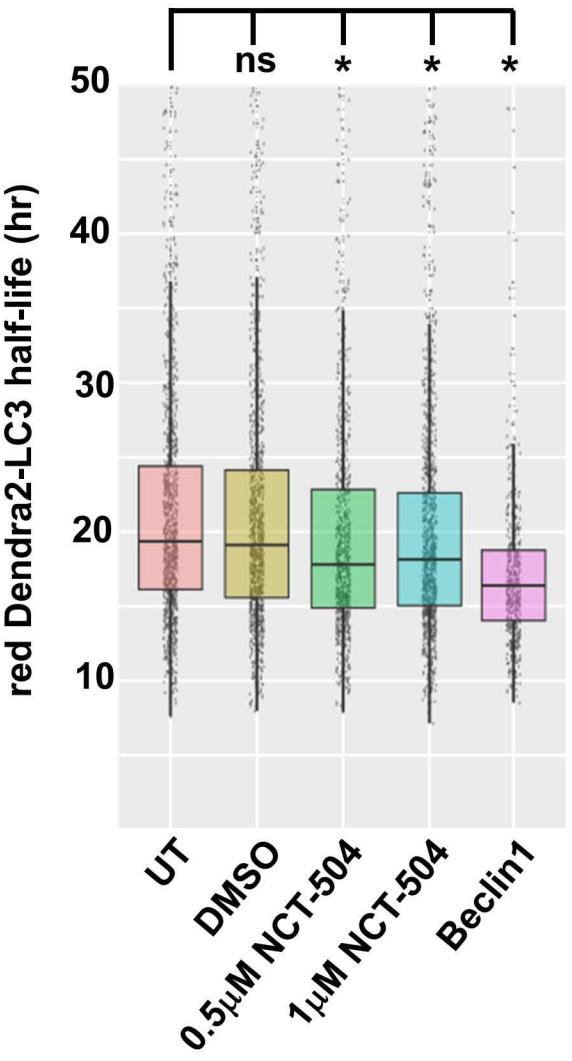

Figure 3 – figure supplement 3

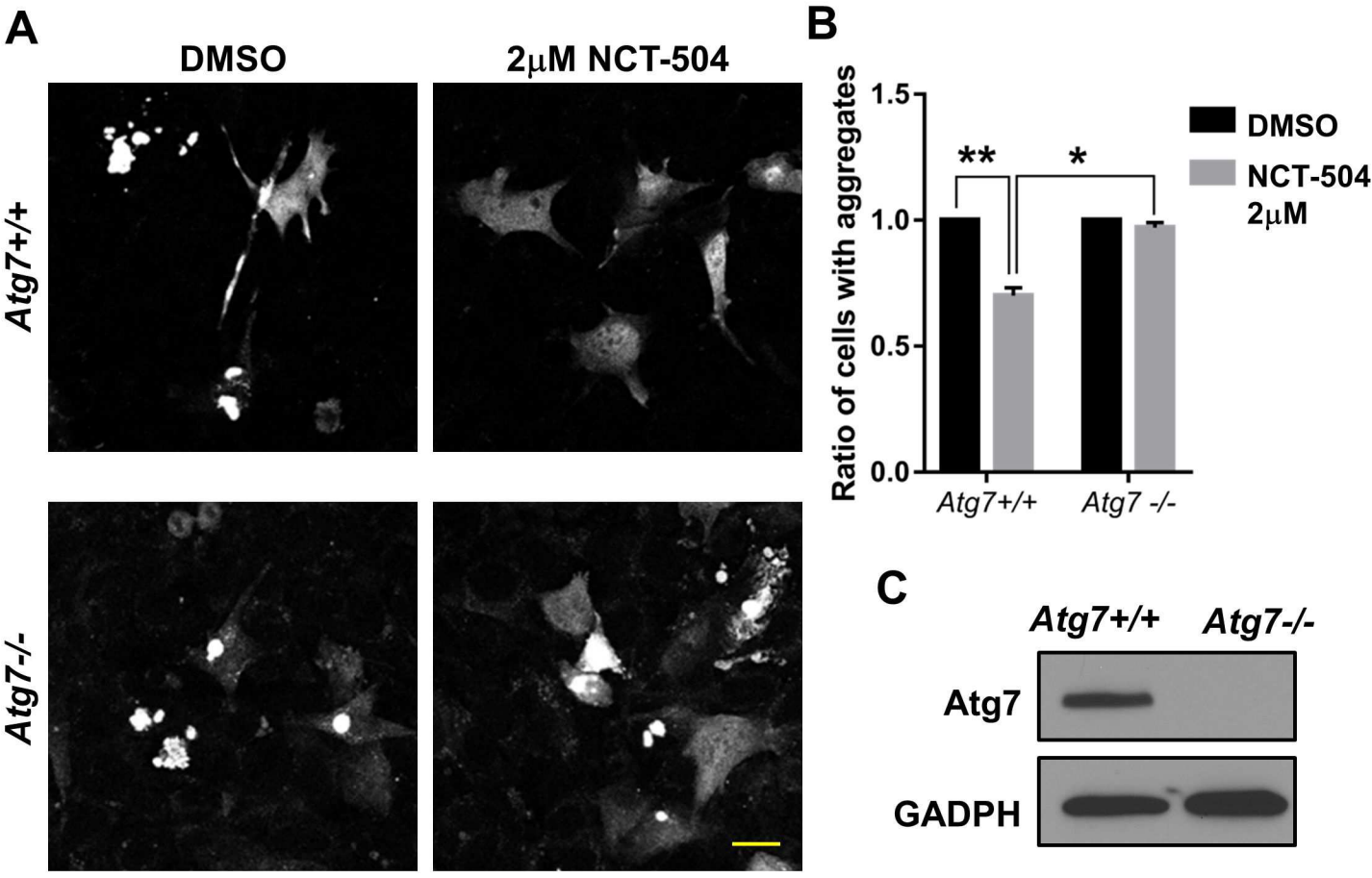

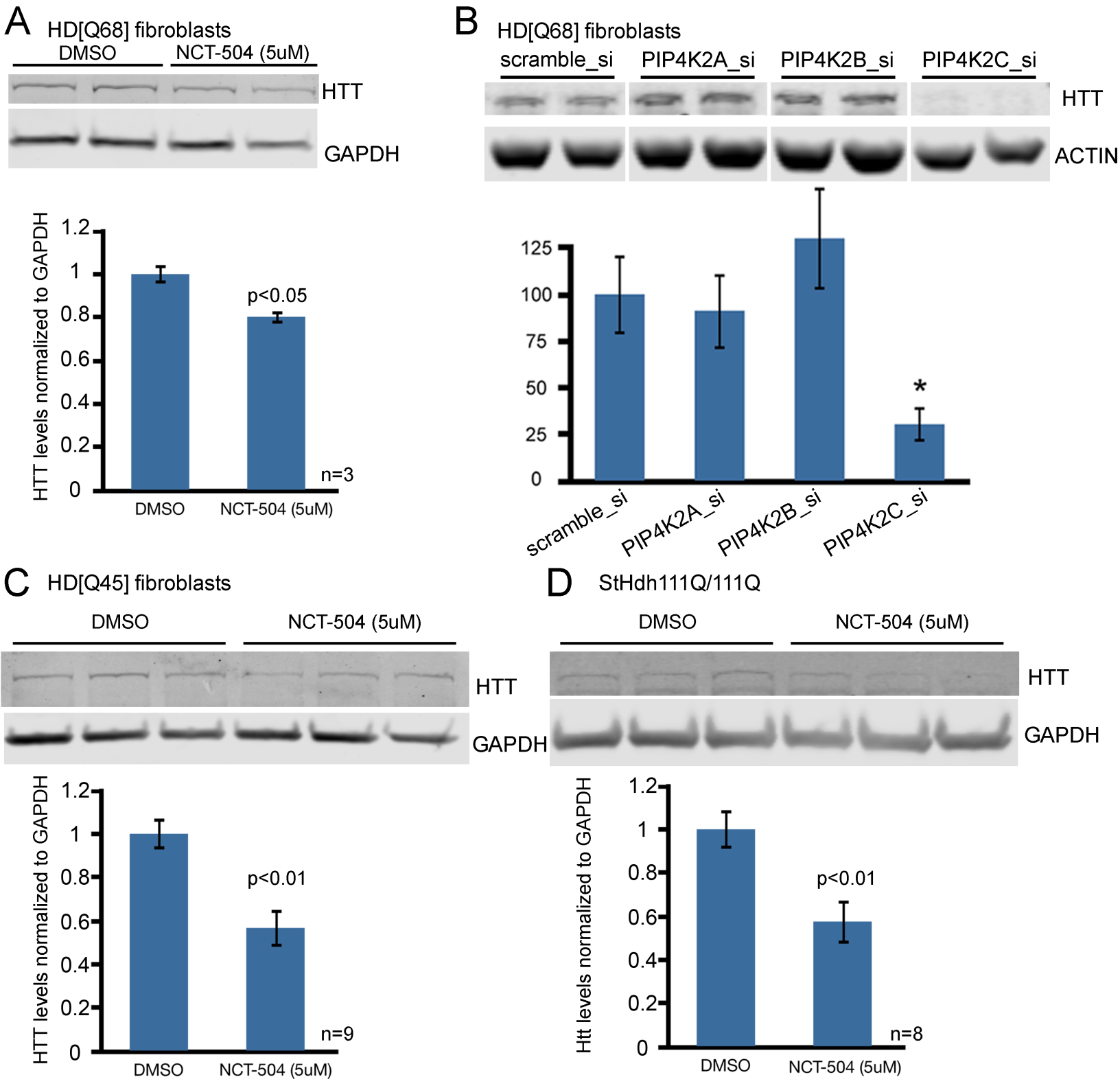
A
HD[Q68] fibroblasts
DMSO
NCT-504 (5uM)
HTT
GAPDH
HTT levels normalized to GAPDH
1.2
1
0.8
0.6
0.4
0.2
0
p<0.05
n=3
DMSO
NCT-504 (5uM)
B
HD[Q68] fibroblasts
scramble_si
PIP4K2A_si
PIP4K2B_si
PIP4K2C_si
HTT
ACTIN
125
100
75
50
25
0
*
scramble_si
PIP4K2A_si
PIP4K2B_si
PIP4K2C_si
C
HD[Q45] fibroblasts
DMSO
NCT-504 (5uM)
HTT
GAPDH
HTT levels normalized to GAPDH
1.2
1
0.8
0.6
0.4
0.2
0
p<0.01
n=9
DMSO
NCT-504 (5uM)
D
StHdh111Q/111Q
DMSO
NCT-504 (5uM)
HTT
GAPDH
Htt levels normalized to GAPDH
1.2
1
0.8
0.6
0.4
0.2
0
p<0.01
n=8
DMSO
NCT-504 (5uM)

Figure 4 – figure supplement 1

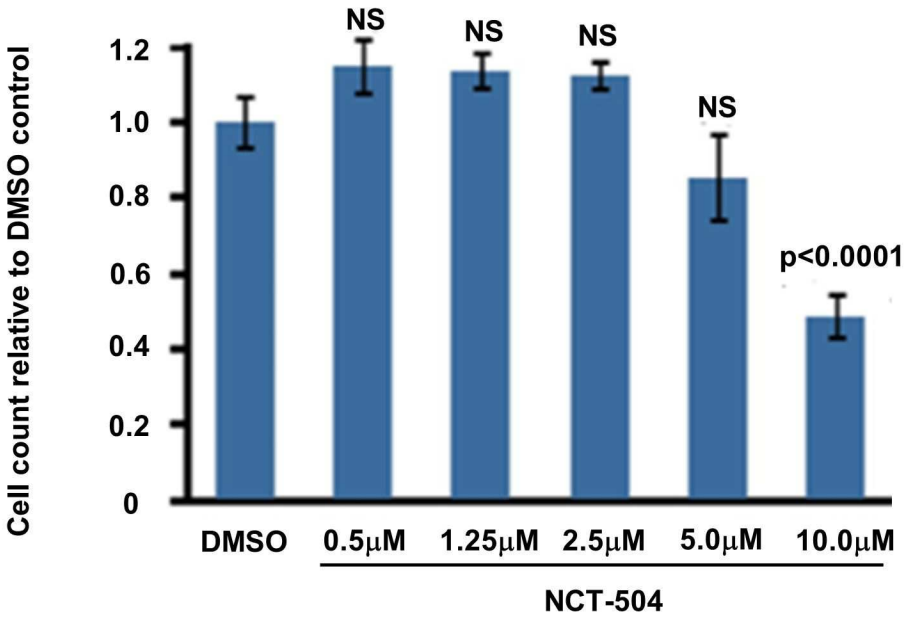

Figure 4 – figure supplement 2

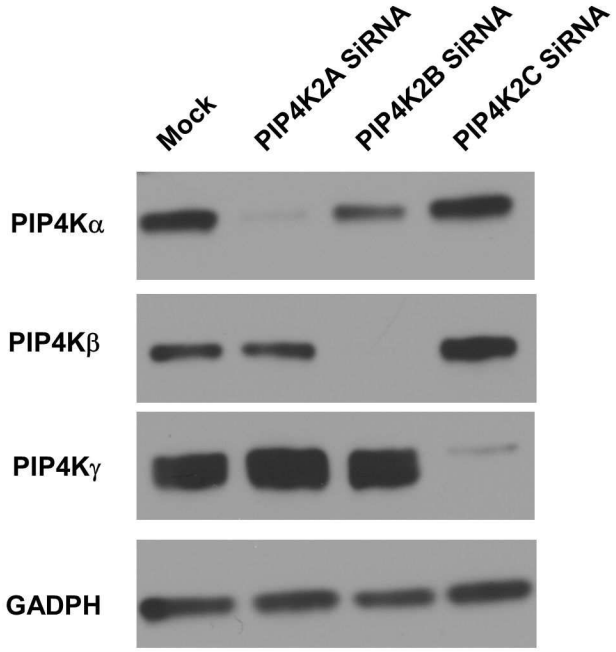

Figure 4 – figure supplement 3

A

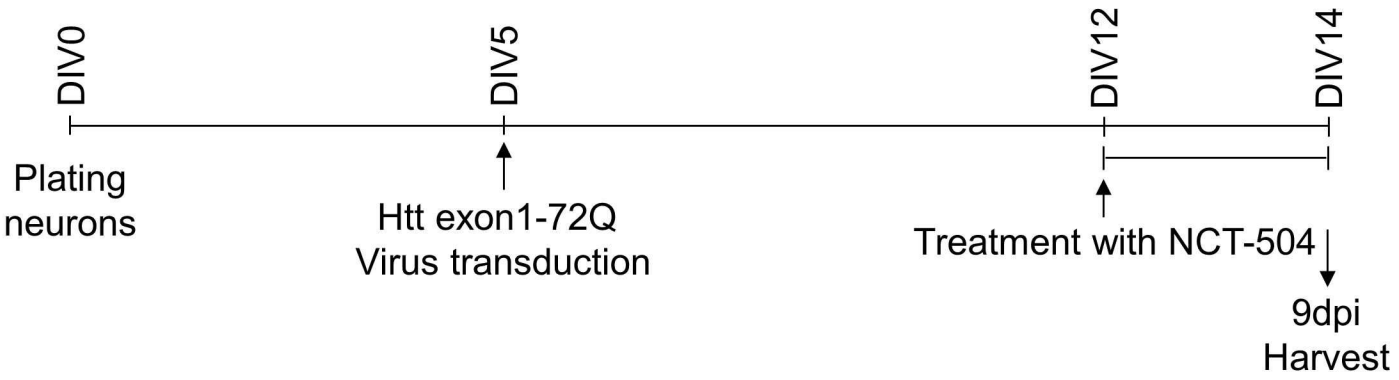

B

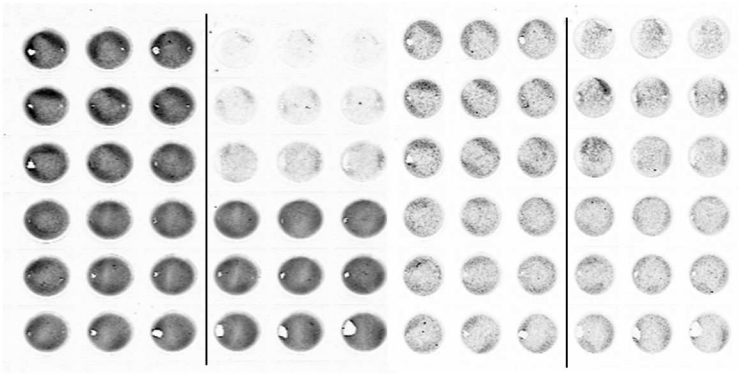

veh (50μM)	NCT-504 (50μM)
veh (20μM)	NCT-504 (20μM)
veh (10μM)	NCT-504 (10μM)
veh (5μM)	NCT-504 (5μM)
veh (2.5μM)	NCT-504 (2.5μM)
veh (1.25μM)	NCT-504 (1.25μM)

Figure 4 – figure supplement 4

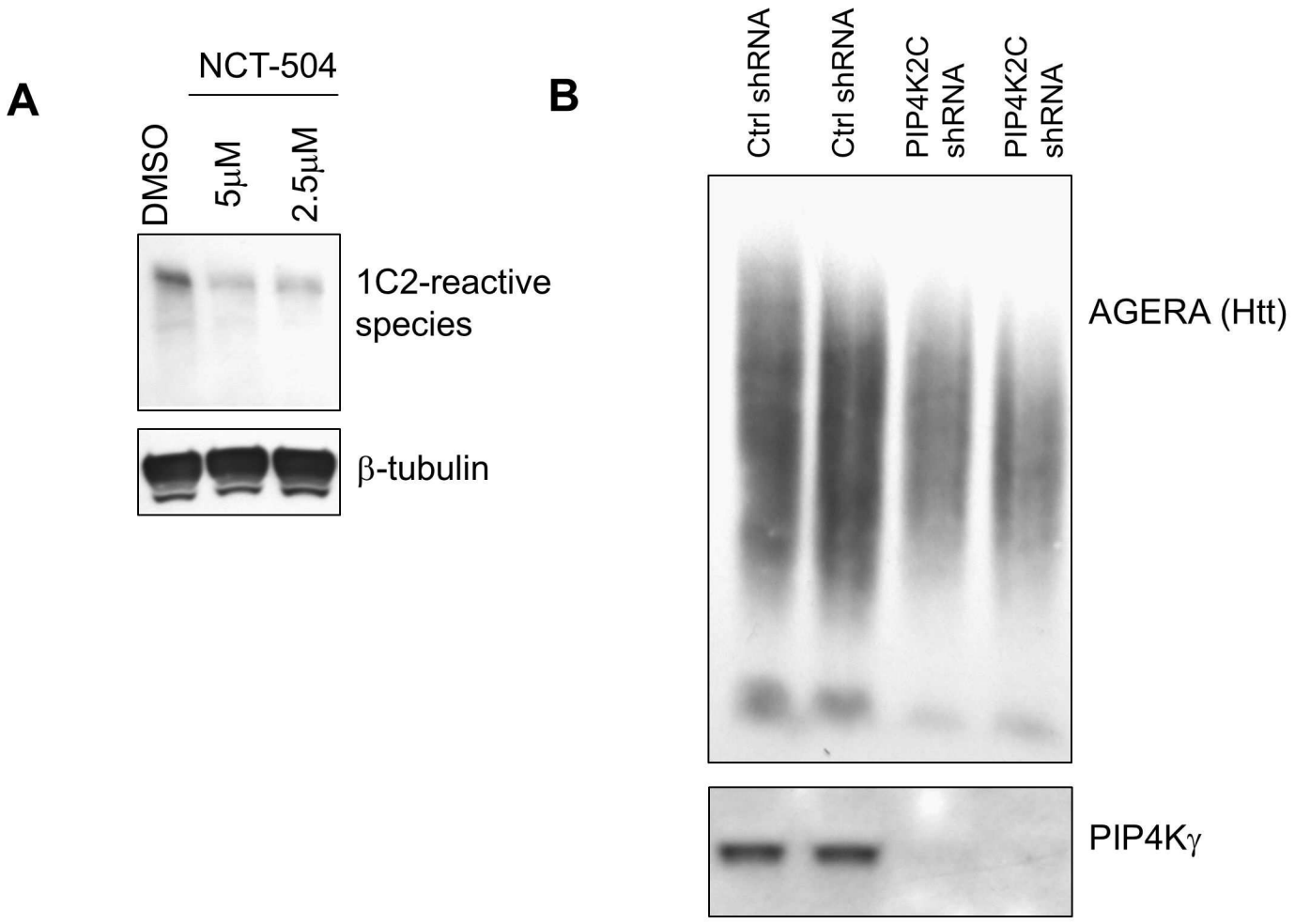

Figure 4 – figure supplement 5

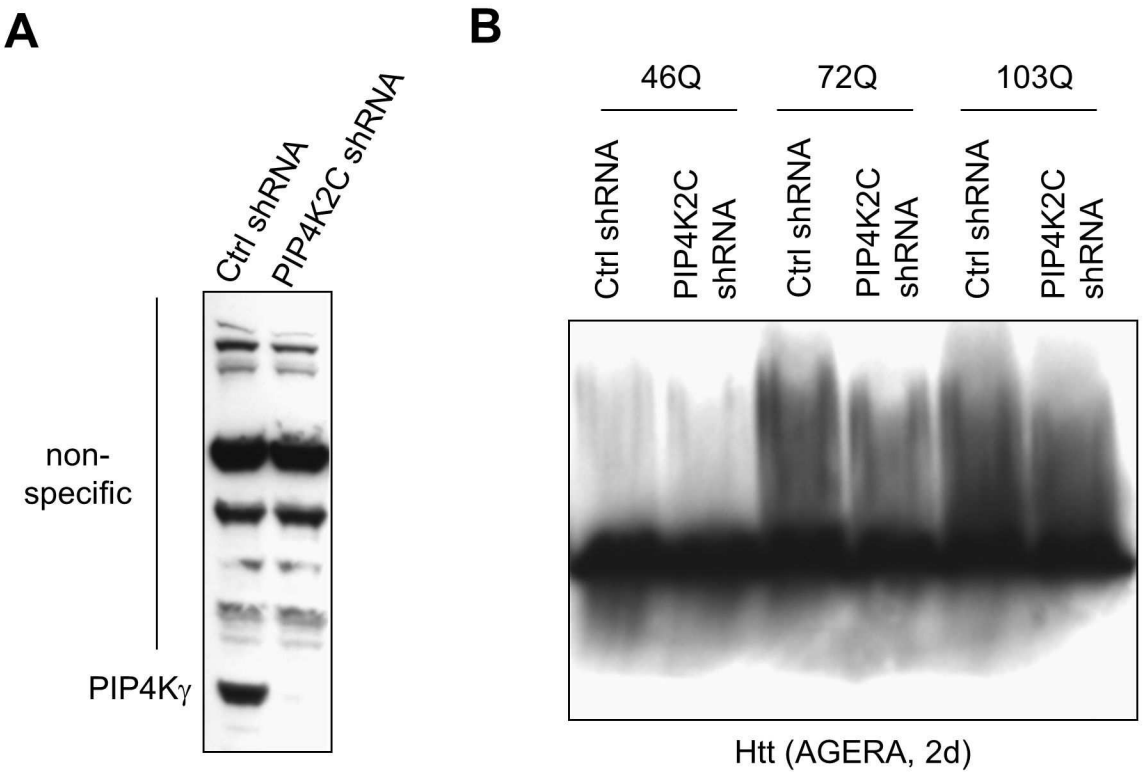

Figure 5

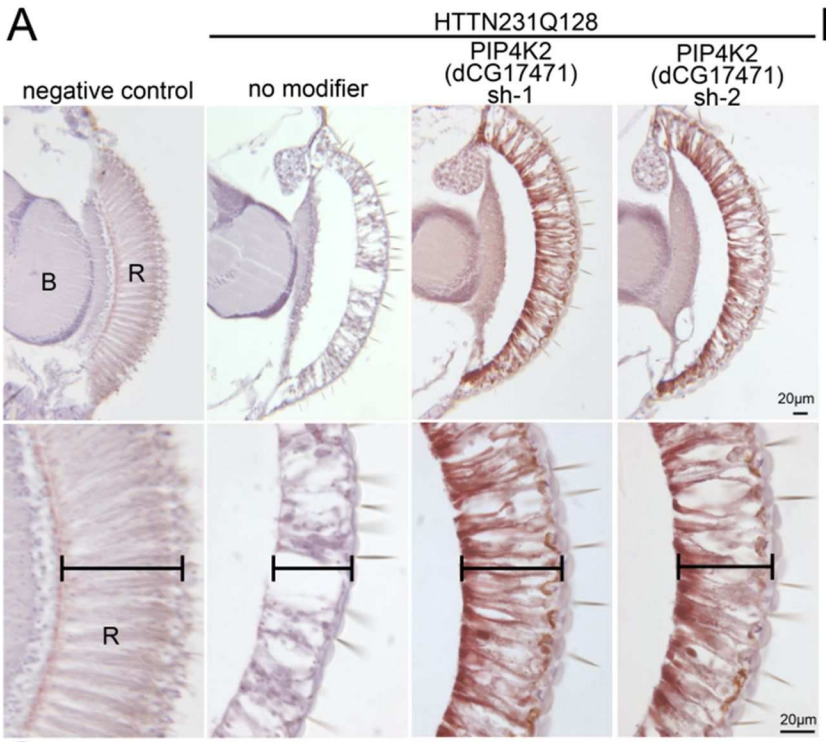
A
HTTN231Q128
negative control
no modifier
PIP4K2 (dCG17471) sh-1
PIP4K2 (dCG17471) sh-2
B
R
20μm
R
20μm

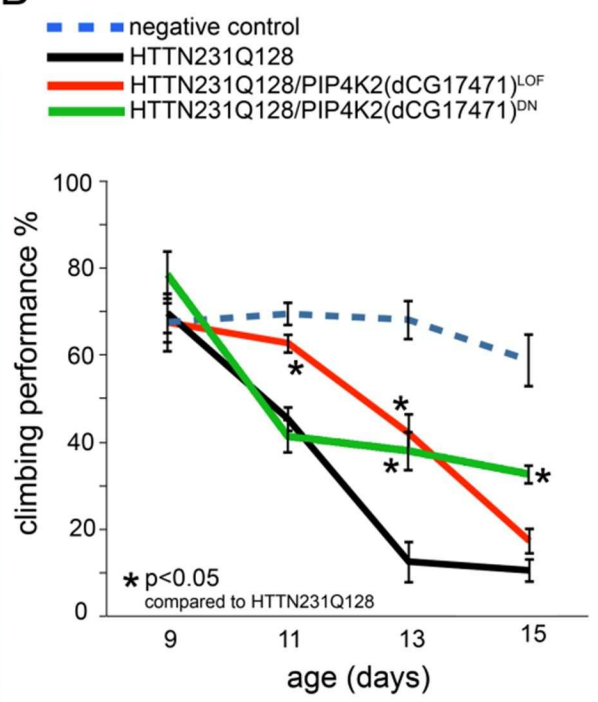
B
negative control
HTTN231Q128
HTTN231Q128/PIP4K2(dCG17471)LOF
HTTN231Q128/PIP4K2(dCG17471)DN
climbing performance %
100
80
60
40
20
0
* p<0.05
compared to HTTN231Q128
9
11
13
15
age (days)

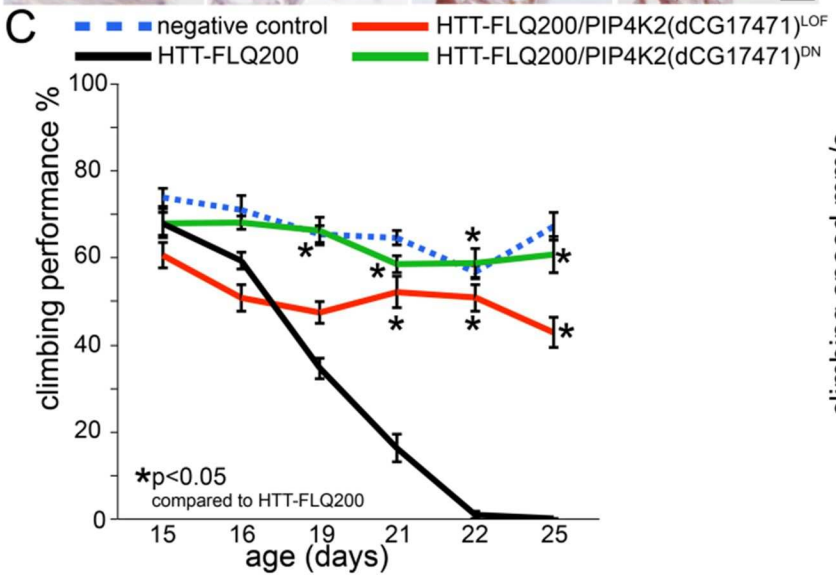
C
negative control
HTT-FLQ200
HTT-FLQ200/PIP4K2(dCG17471)LOF
HTT-FLQ200/PIP4K2(dCG17471)DN
climbing performance %
100
80
60
40
20
0
*p<0.05
compared to HTT-FLQ200
15
16
19
21
22
25
age (days)

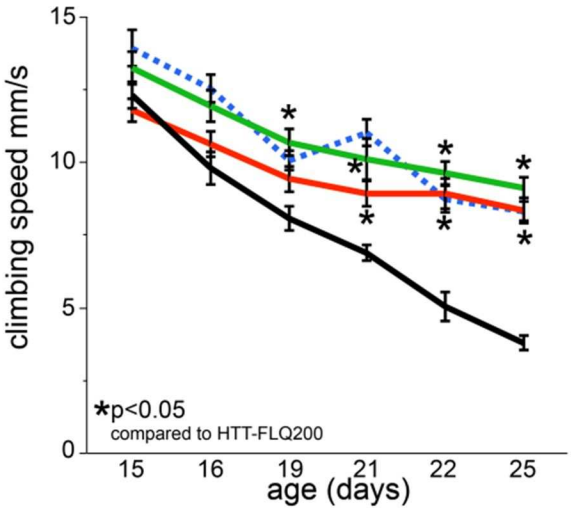
climbing speed mm/s
15
10
5
0
*p<0.05
compared to HTT-FLQ200
15
16
19
21
22
25
age (days)

Figure 5 – figure supplement 1